Cognitive Radio Connectivity for Railway Transportation Networks

by

Kuldeep S. Gill

A Thesis
Submitted to the Faculty
of the
WORCESTER POLYTECHNIC INSTITUTE
in partial fulfillment of the requirements for the
Degree of Master of Science
in
Electrical and Computer Engineering
by

December 2017

APPROVED:

Professor Alexander Wyglinski, Major Advisor

Professor Kaveh Pahlavan

Dr. Travis Collins

Abstract

Reliable wireless network for high speed trains requires a massive amount of data communications for enabling safety features such as train collision avoidance and railway management. Cognitive radio integrate heterogeneous wireless networks that will be deployed in order to achieve intelligent communications in future railway systems. One of the primary technical challenges in achieving a reliable communication for railways is the handling of high mobility of trains, which includes the high Doppler shifts in the transmission as well as the severe fading environment that makes it difficult to estimate wireless spectrum utilization. This thesis has two primary contributions: (1) Heterogeneous Cooperative Spectrum Sensing (CSS) prototype system, and (2) Long Term Evolution for Railways (LTE-R) performance analysis. The Heterogeneous CSS prototype system was implemented using Software-Defined Radios (SDRs) possessing different radio configurations. Both soft and hard data fusion schemes were used in order to compare the signal source detection performance in real-time fading scenarios. For future smart railways, the most effective solution is to use the underutilized spectrum as a secondary user via dynamic spectrum access (DSA). Since it is challenging to get an accurate estimate of incumbent users with a single-sensor system under a practical fading environment, the proposed cooperative spectrum sensing approach is employed instead since it can mitigate the effects of multipath and shadowing by utilizing the spatial and temporal diversity of a multiple radio network. Regarding the LTE-R contribution of this thesis, the performance analysis of high speed trains (HSTs) in tunnel environments would provide valuable insights with respect testing to the smart railway systems operating in high mobility scenarios in drastically impaired channels.

Acknowledgements

I would like to express my deepest gratitude to my advisor Professor Alexander Wyglinski for his continuous guidance and support towards my degree. I am very thankful for the opportunity to work with him in the Wireless Innovation Laboratory at Worcester Polytechnic Institute.

I want to thank Professor Kaveh Pahlavan and Dr. Travis Collins for serving on my committee and providing valuable suggestions and comments with regards to my thesis. I would also like to thank my WILab team members Dr. Srikanth Pagadarai, Dr. Paulo Ferreira, Renato, Le for their immense support during my graduate studies. And I would also like to thank my friends Rasika, Devdip and Raunak for their constant emotional support. Finally, I'm also thankful to my parents, without their constant support I wouldn't be here.

Contents

List of Figures

List of Tables

Chapter 1

Introduction

1.1 Motivation

Gradually we are moving towards context awareness among automotive devices where the vehicles are aware of their neighborhood. In modern railway applications, a huge amount of wireless communications is used for safety features such as train collision avoidance and railway management. To enhance reliability and safety of Railway systems, while increasing accessibility and productivity, modern railway operations rely on an ever increasing amount of exchange of information between different trains, i.e., train-to-train (T2T) and train-to-ground (T2G). The integration of all of these heterogeneous wireless networks deployed in the railway domain constitutes a key technical challenge. These challenges can potentially be answered by Cognitive Radio (CR) technologies, which can offer interoperability, reliability, dynamic spectrum access, and both lower deployment and maintenance costs. Two research projects currently underway for cognitive radio enabled railway communication include the following:

- Cognitive Radio for Railway Through Dynamic and Opportunistic Spectrum Reuse (CORRIDOR) [4] is a French research project that targets opportunistic spectrum access for railways. Due to the rapid increase in demand for future railways in terms of control operations as well as providing high speed internet connectivity to the passengers, more bandwidth and spectrum is needed for railway communications.

- Rail-CR project [5] is a US-based railway system project where the main effort is focused on implementing a positive train control (PTC) technology designed to equip trains with wireless communication capabilities. The project aims to allow trains to communicate with wayside wireless stations while moving to supply important information such as speed and direction in order to improve safety and operations of the railway system.

In this thesis, we have designed and implemented two prototypes to further the advancement of smart railway communication systems. In the first test-bed, we have analyzed the performance of high speed train (HST) systems in a tunnel environment. In recent years, the use of trains have witnessed tremendous growth due to their high speeds, which has led to the demand for reliable wireless communication systems with these transportation systems. The development of a reliable wireless network for high speed trains is not a simple task and it is still an emerging technology. Global System for Mobile Communication for Railways (GSM-R) [6], was a wireless communications standard designed for high speed trains, but it turned out not to be reliable enough and possess several limitations. Subsequently, LTE-R [7] proposed a promising solution for achieving broadband data rates in high speed trains that can overcome various GSM-R limitations [8, 9].

LTE-R is a high speed communication standard based on the existing LTE system architecture [9]. There has been several studies regarding the assessment of LTE-R as a viable choice for next generation high speed communications for railway applications [10,11]. Most LTE systems operate at 1.8 GHz – 2.6 GHz bands, which possesses a high propagation loss and severe fading effects. Highly mobile trains inside tunnel environments makes the design of reliable communication links very challenging. To achieve reliable radio coverage inside tunnels, leaky feeder cables have been proposed [12]. With LCX, more uniform coverage can be achieved and installation is also comparatively simple. Each slot in the cable is equivalent to an antenna, which can transmit and receive signals. Figure 1.1 shows the LOS propagation environment inside a tunnel for a high speed train with velocity v.

The second proposed contribution of this thesis is the design and implementation of a GNU Radio based software-defined radio network performing cooperative spectrum sensing.

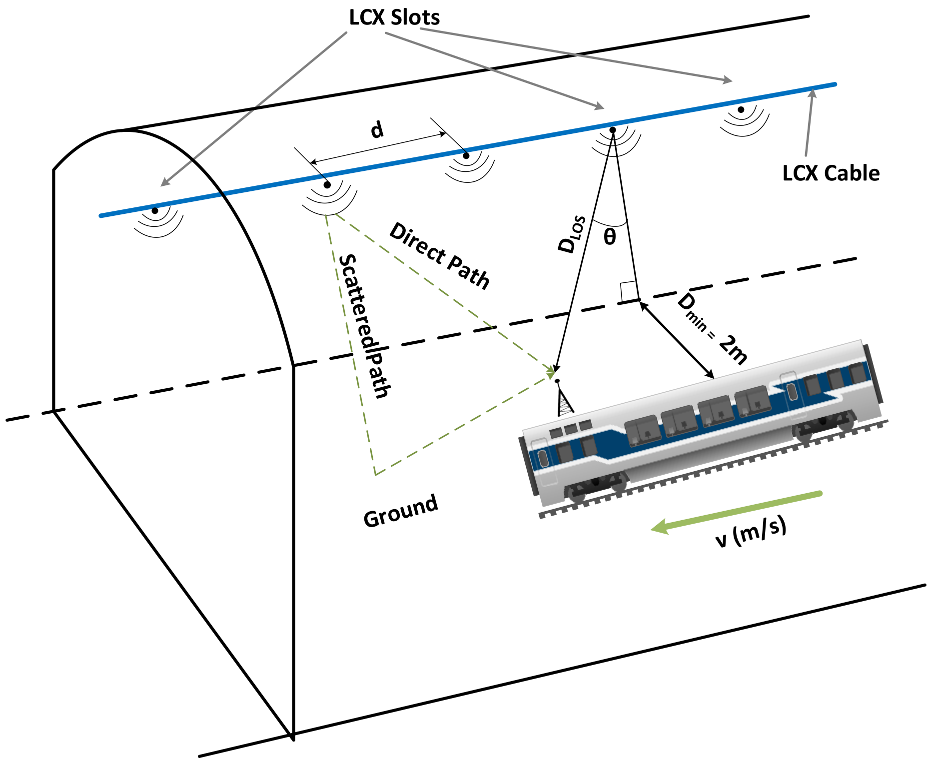

Figure 1.1: High speed train inside a tunnel for LTE-R. D_{LOS} is the distance between transmitter and receiver, d is the distance between the LCX cable transmission slots.

Smart railway communication system requires large bandwidth in order to support the high data-rate applications. This has facilitated the research in dynamic spectrum access (DSA) [13, 14] for efficient utilization of spectrum resources to sustain billions of Internet of Things (IoT) devices. There has been a significant increase in the study of cognitive radios for efficiently utilizing the electromagnetic spectrum. It has been observed that the spectrum occupancy is not uniform across all frequency bands, resulting in numerous spectral white spaces [3]. To opportunistically access these idle channels, spectrum sensing is considered to be a significant technology for enabling DSA. Although several spectrum sensing techniques have been proposed in the open literature, energy detection is widely used due to its low implementation complexity [15]. We discuss some of the spectrum sensing techniques along with energy detection below:

- In *energy detection* (ED), the energy of the signal is detected in the frequency location and based on the threshold value we decide whether the signal is present or absent.

- *Cyclostationary Feature Detection* is a complex scheme to implement compared to ED and it is mostly used when we need to also classify the signal present based on their modulation scheme.

- When secondary user has *apriori* knowledge of primary user signal, *matched filter* (MF) detection is applied. Detection by using matched filter needs less detection time compared to ED but primary user information is required.

These spectrum sensing techniques can be used in a non-cooperative manner but it is very challenging to get an accurate estimate using a single-sensor system within a practical fading environment. Various non-idealities, such as shadowing, multipath, and fluctuating noise variance, can make it difficult to detect the primary user [16,17]. Cooperative spectrum sensing can mitigate the effects of multipath and shadowing by utilizing the spatial and temporal diversity of a multiple radio network [18, 19]. In cooperative spectrum sensing, each sensor node collects the spectral data and transmits it to a fusion center (FC) for decision making. Figure 1.2 shows how a heterogeneous sensor network exploits the spatial diversity.

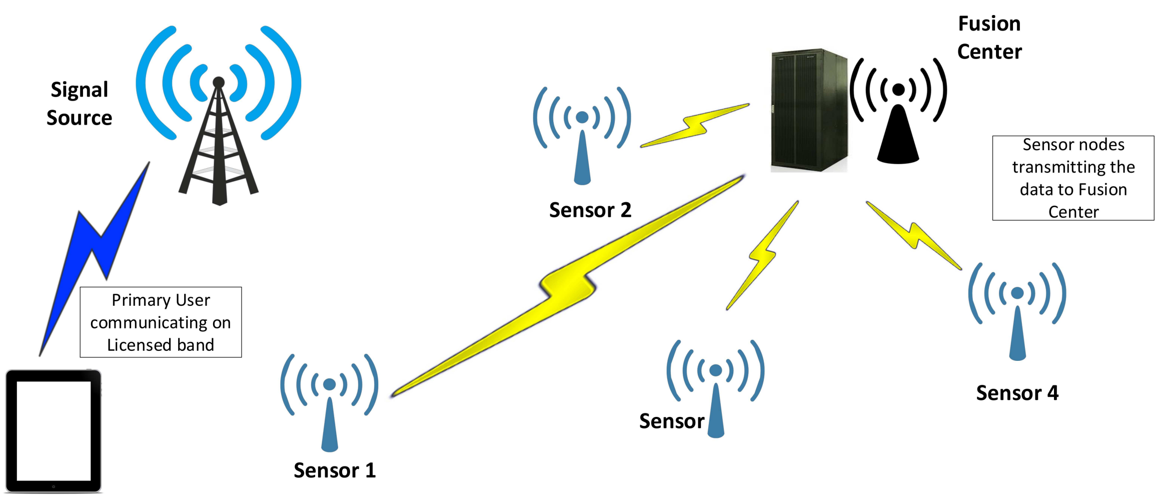

Figure 1.2: Heterogeneous sensor network employing cooperative spectrum sensing. $RFFE_i$ and SR_i represents different front end and sampling rates for the SDR units.

1.2 State of the Art

In the open literature, most channel modeling techniques have considered open areas for high speed trains [10,11], while relatively little research has been conducted for trains operating in tunnel environments. Due to various challenges presented by tunnel environments, it is important to derive a channel model for LTE-R involving high speed trains. In this thesis, we analyze the effects of high Doppler shift and multipath propagation due to tunnel environments. Experimental studies conducted inside tunnel environments have shown that the field amplitude distribution fits smoothly over a Rician distribution [20]. Several research efforts have been conducted for large-scale and small-scale fading characteristics for wideband communication systems inside tunnel environments. To the best of the authors knowledge, none of these studies have been conducted for LTE-R, which employs Orthogonal Frequency Division Multiplexing (OFDM) signals for data transmission inside tunnels. The large Doppler shifts caused by high speed trains will potentially lead to ambiguity when extracting the carrier frequency, which can potentially increase the BER [21]. Therefore, it is important to study the effects of high Doppler shift and multipath fading for LTE-R communications in tunnel environments such that equalizers can be design efficiently.

The cooperative spectrum sensing testbed using normalized energy detection has been implemented and and compared with both soft and hard data fusion schemes. Both soft data fusion and hard data fusion have been extensively studied in the literature [22–24], with several algorithms being implemented for each scheme. In a hard decision approach, each local decision statistic from a sensor node is transmitted to an fusion center (FC) via overhead channels. The FC merges the sensing data and makes a global decision based on various algorithms such as majority rule, OR rule, and AND rule [25]. For a soft decision scheme, each sensor unit (SU) sends its local sensing data to the FC, which makes decision based on a global test statistic G. Soft decision combining improves the cooperative gain but it also possesses several limitations. With an infinite bandwidth, the real floating values can be transmitted to the FC, which can lead to a reliable decision mechanism. However, due to bandwidth constraints we have to quantize the data and this leads to error in the energy values. In hard decision combining, we can just transmit the decisions of the sensor nodes to the FC, which can be binary values where "1" indicating that signal source is present and "0" indicating that a signal source is absent.

1.3 Thesis Contributions

This thesis possesses the following contribution to the cognitive radio communications and railway communications field:

- A performance assessment and simulation of LTE-R communications in a tunnel environment experiencing severe fading.
- Dynamic K-factor for a tunnel environment is derived using the classical two-ray propagation model [26] and is used to build Rician fading model for the tunnel.
- A cooperative spectrum sensing hardware prototype with normalized energy detection using both soft data fusion and hard data fusion implemented on available software defined radios.
- For soft data fusion, Maximum Normalized Energy (MNE) and Equal Gain Combination (EGC) algorithms are used. Hard data fusion is also implemented using majority rule, AND, and OR approaches. Both USRP N210s [27] and RTL-SDRs [28] are employed for the implementation of the heterogeneous sensor network.

1.4 Thesis Organization

This thesis is organized into the following chapters: Chapter 2 discusses the smart railway communication system in detail and provides necessary understanding of LTE-R communication system, positive train control (PTC), wireless broadband (WiBro), spectrum regulation. Chapter 3 provides background knowledge on heterogeneous cooperative spectrum sensing and focuses on heterogeneous networks, cooperative spectrum sensing, and software-defined radios. Chapter 4 discusses the proposed LTE-R implementation and its results in a tunnel environment. Channel impairments and two-ray propagation model are also discussed in details. In Chapter 5, the proposed implementation of a heterogeneous cooperative spectrum sensing (CSS) test-bed and results are discussed. Chapter 6 concludes this thesis, summarizing the accomplishments and outlines possible future work.

1.5 List of Related Publications

The following publications resulted from the activities of this thesis research:

- K. S. Gill and A. M. Wyglinski, "Heterogeneous Cooperative Spectrum Sensing Test-Bed Using Software-Defined Radios," in Vehicular Technology Conference (VTC Fall), 2017 IEEE 86th, Sept 2017.
- K. S. Gill, P.V.R Ferreira and A. M. Wyglinski, "Performance Analysis of High Speed Railways Communications Inside a Tunnel Using LTE-R," in Vehicular Technology Conference (VTC Fall), 2017 IEEE 86th, Sept 2017.

Chapter 2

Smart Railway Communication System

With the rapid development of the high speed railways (HSRs) communication system, it is more convenient for people to travel by train. The huge demand in HSR travel has led to huge growth in next generation wireless communication systems. Current GSM-railway (GSM-R) technology is not sufficient for satisfying the demand for large data rate applications and quality-of-service (QoS), which has consequently led to development of Long Term Evolution for railways (LTE-R). LTE-R is based on the LTE architecture and has been championed as future of the smart railway communication system. LTE-R provides a more efficient network architecture compared to GSM and has a reduced packet delay. It is also based on a well-established and off-the shelf communication system that provides standardized interworking mechanisms and compatibility with GSM-R. In the following section, we discuss positive train control (PTC), wireless broadband (WiBro), train-to-train (T2T), and train-to-ground (T2G) communication, Long Term Evolution for Railways (LTE-R) communication system, spectrum regulation for railway communication systems, LTE-R services for railways and leaky coaxial cable (LCX), which are important technologies for achieving smart railway transportation system, will also be discussed.

2.1 Positive Train Control

Positive Train Control (PTC) is designed for monitoring and controling of train movements in order to provide advanced safety with the help of modern wireless communication technology. The key idea behind PTC is the constant flow of information to the train about its location, warnings if engineer does not slow down the train, derailments caused by excessive speed of train, etc. Managing track occupancies through centralized route and interlocking logic, enforcing permanent and temporary speed limits for the train, and real-time localization of the train are some of the basic features implemented in PTC.

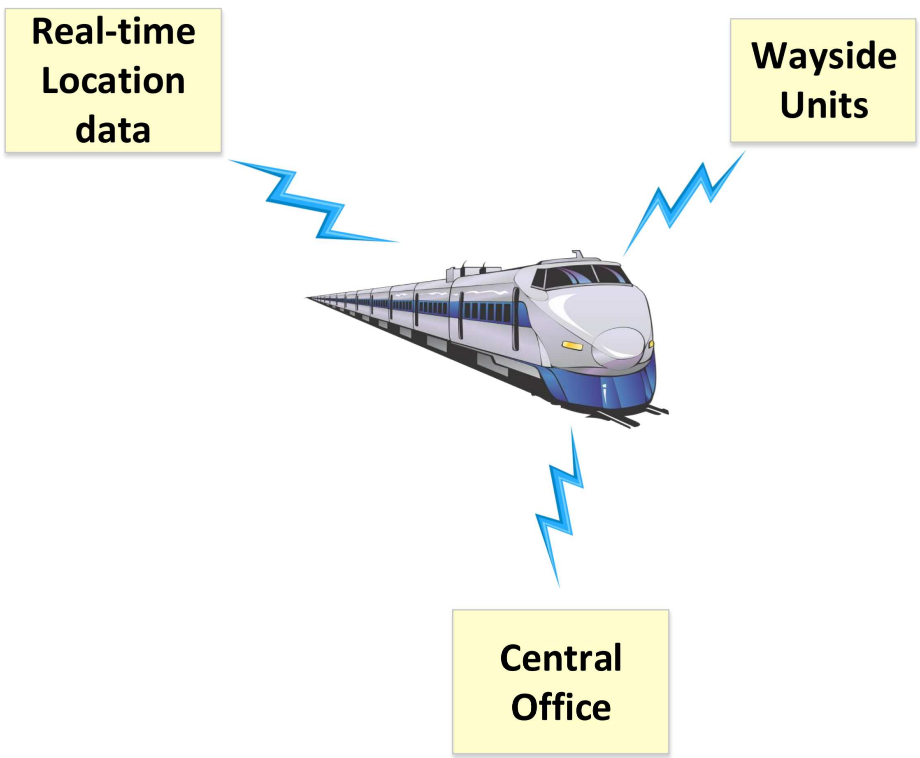

Figure 2.1: Architecture of Positive Train Control consisting of wayside units, central office and real-time GPS information. All these technologies assist PTC in achieving advance control and safety of the trains.

Figure 2.1 gives a simplistic viewpoint of the PTC architecture; where the train receives the flow of information through various system using wireless communication links. The primary means of determining location for the train is by using differential GPS, which can continuously compare its position with the stored position of speed restriction and work zones [29]. The Central Office (CO) regularly monitors trains, exchanging information with Train management computers (TMC) and gathering precise speed and position information. The CO also collects information regarding train orders, number of cars, weight, route and track characteristics along the route, including speed restrictions, curves, grades and crossing. All wayside equipment are continuously monitored by PTC, where they issue alerts in cases when an automatic crossing gate is not working or a hot box detector senses several axles slightly above a certain temperature level. It also applies corrective action in cases where there are reports of a possible track breakage due to extreme heat or a flood.

2.2 Wireless Broadband (WiBro)

Wireless Broadband (WiBro) is a mobile broadband wireless access (BWA) service which had its first public demonstration in December 2005 and has been in service in South Korea since June 2006. WiBro was developed as a mobile BWA solution in Korea and was based on the IEEE 802.11e WiMax standard. It is a subset of the consolidated version of the IEEE Standard 802.16- 2004 (fixed wireless specifications), P802.16e (enhancements to support mobility), and P802.16-2004/Cor1 (corrections to IEEE Standard 802.16-2004). The profiles and test specifications of WiBro have been harmonized with the WiMAX Forum's mobile WiMAX profiles and test specification, resulting in a convergence of the two standards.

Figure 2.2 describes the architecture of BWA-based WiBro communication system in the Phase I standardization [30]. The WiBro network consists of Access Control Routers (ACR), which connects the backbone network with Radio Access Station (RAS). The RAS is the interface between mobile nodes and the core network at the physical layer and it controls the radio resource at the data link layer in conjunction with an ACR. The key distinction of WiBro from conventional cellular networks is that the Internet Protocol (IP) is used between an ACR and RASs, as well as between ACRs. WiBro uses Time Division Duplexing (TDD) or Frequency Division Duplexing (FDD) for duplexing and Orthogonal Frequency Division Multiple Access (OFDMA) for robustness against fast fading and narrow-band co-channel interference.

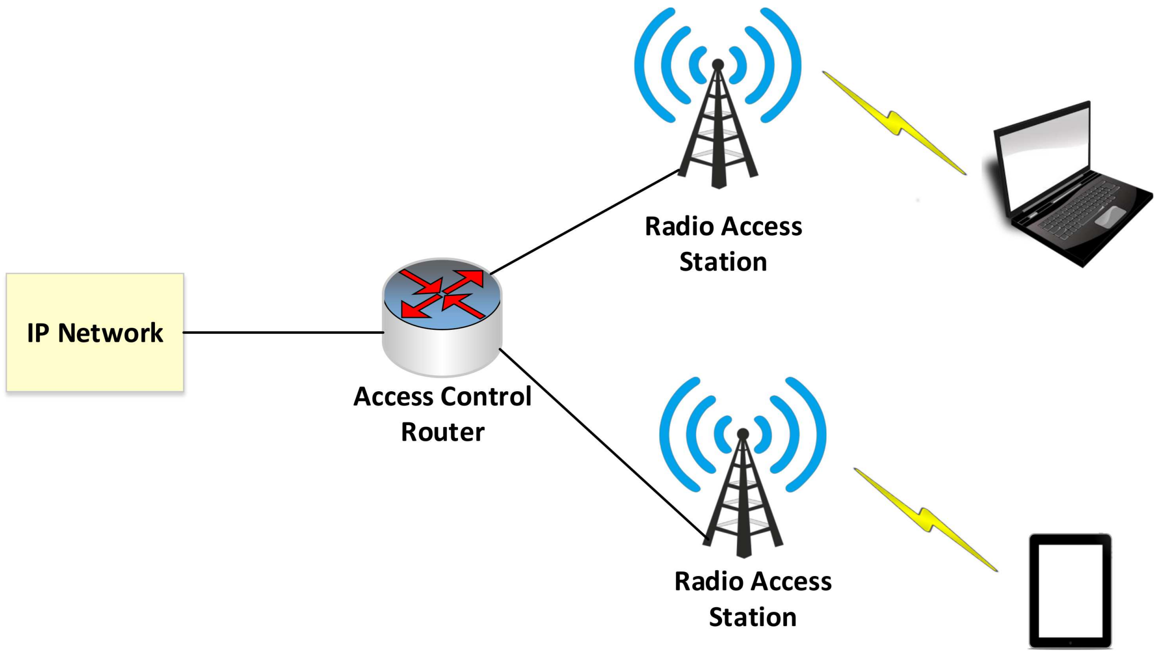

Figure 2.2: Korean Wireless Broadband (WiBro) system architecture for high speed internet connectivity. WiBro is an all IP-based network, which uses ACRs to connect the backbone network with radio access station.

2.3 LTE-R Communication System

The development of a reliable wireless network for high speed trains is not a simple task and it is still an emerging technology. Global System for Mobile Communication for Railways (GSM-R) [6] was a wireless communications standard designed for high speed trains, but it turned out not to be reliable enough and possessed several limitations. The data rates for voice services, which can reach up to 9.6 kbps, was unable to meet the increasing demands of high-rate data transmission for railways communication. Furthermore, the limited data rate and quality of service (QoS) requirements where not enough to support cellular communications. Subsequently, LTE [7] proposed a promising solution for achieving broadband data rates, flexible bandwidth allocation, and high spectral efficiency in high speed trains that can overcome various GSM-R limitations [8, 9].

LTE-R is a high speed communication standard based on the existing LTE system architecture [9]. There has been several studies regarding the assessment of LTE-R as a

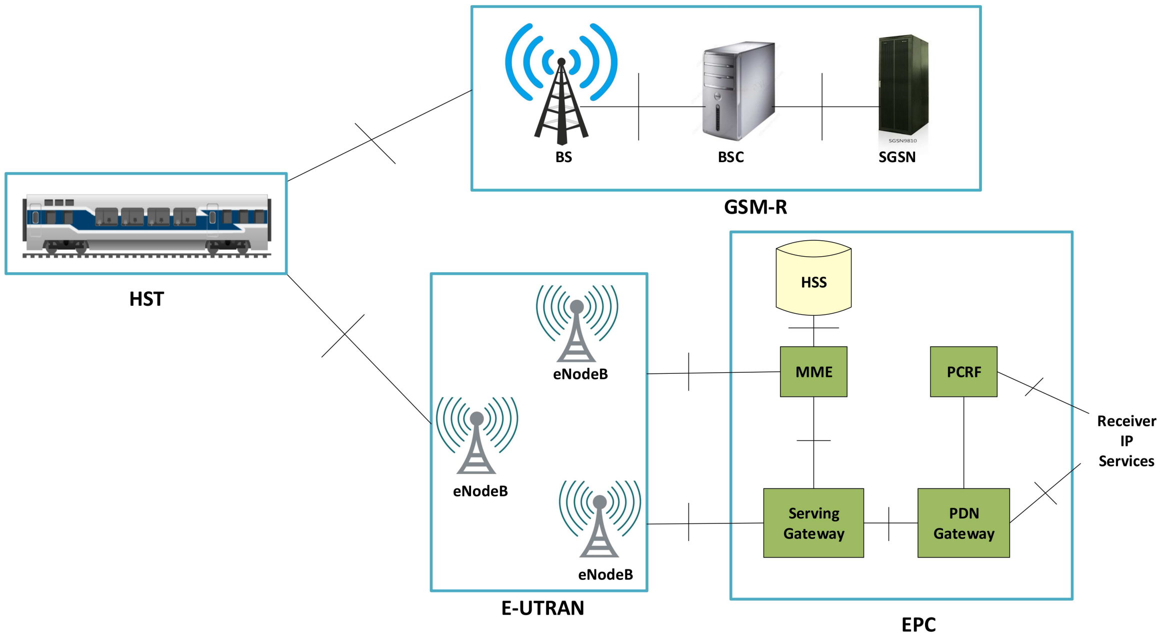

Figure 2.3: Proposed LTE-R Architecture for next generation High-speed Railways consisting of EPA and E-UTRAN.

viable choice for next generation high speed communications for railway applications [10,11]. Conventional LTE includes an Evolved Packet Core (EPC) network and a radio access network referred to as an Evolved Universal Terrestrial Radio Access Network (E-UTRAN). The Internet Protocol (IP)-based EPC supports seamless handovers for both voice and data to cell towers, and each E-UTRAN cell will support high data and voice capacity by high-speed packet access (HSPA). As a candidate for the next-generation communication system of HSR, LTE-R inherits all the important features of LTE and provides an extra radio access system to exchange wireless signals with onboard units (OBUs) and to match HST-specific needs. Figure 2.3 shows the proposed architecture of LTE-R according to [7], and it shows that the core network of LTE-R is backward compatible with GSM-R. The network architecture of LTE-R is similar to that of LTE/SAE, with Evolved Universal Terrestrial Radio Access Network (E-UTRAN) being the access network structure of LTE-R. The Evolved-Node B (eNodeB) units communicate directly with UEs similar in fashion to a base transceiver station (BTS) in GSM networks. It performs the transmission and reception of data packets using Orthogonal Frequency Division Multiplexing Access (OFDMA) for downlink and Single Carrier Frequency Division Multiple Access (SC-FDMA) for uplink across the PHY layer. At the same time, as without the base-station controller (BSC), it also has functions of radio resource control and wireless mobility management. The eNodeB units can be connected to the network router directly without more intermediate control nodes, such as the BSC in GSM-R [31]. The significant difference between EPC and the core network of GSM-R is that the EPC is an all-IP mobile core network.

Table 2.1: Comparison of system parameters between GSM-R , LTE and LTE-R.

System Parameters	GSM-R	LTE	LTE-R
Frequency	Uplink: 876–880 MHz downlink: 921–925 MHz	800, 1800, 2600 MHz	450, 800, 1400, 1800 MHz
Capacity	0.2 MHz	1.4-20 MHz	1.4-20 MHz
Modulation	GMSK	QPSK/16-QAM/64-QAM	QPSK/16-QAM
MIMO	No	2x2, 4x4	2x2
Cell Range	8 Km	1-5 Km	4-12 Km
Data Rates (DL/UL)	172/172 Kbps	100/50 Mbps	50/10 Mbps

Conventional LTE networks are different compared to LTE-R in many ways, such as architecture, system parameters, network layout, services, and quality of service (QoS). Table 2.1 summarizes the LTE-R parameters and describe the differences between LTE, GSM-R, and LTE-R. Since the LTE-R environment possesses very severe fading and high Doppler shift, it is configured for QoS rather than higher data rates. Therefore, QPSK modulation is used for most number of subcarriers and the number of packet re-transmissions must be kept low, which is achieved with User Datagram Protocol (UDP).

2.4 Spectrum Regulation for LTE-R

Departing from technical issues for a moment, we now discuss the crucial interactions that smart railways will encounter with respect to spectrum policy and allocation by the Federal Communications Commission (FCC). The spectrum allocated for cellular technologies is already saturated in peak markets due to massive amounts of wireless services and networks. Figure 2.4 shows the pronounced scarcity in the the wireless cellular bands as seen from a frequency allocation chart of the United States. Frequencies at the lower spectrum can be used for wide coverage, mobility support, and control signaling while the high frequencies can be used for high data rate applications. This requires a new approach to spectrum policy and allocation methods for smart railway standardization.

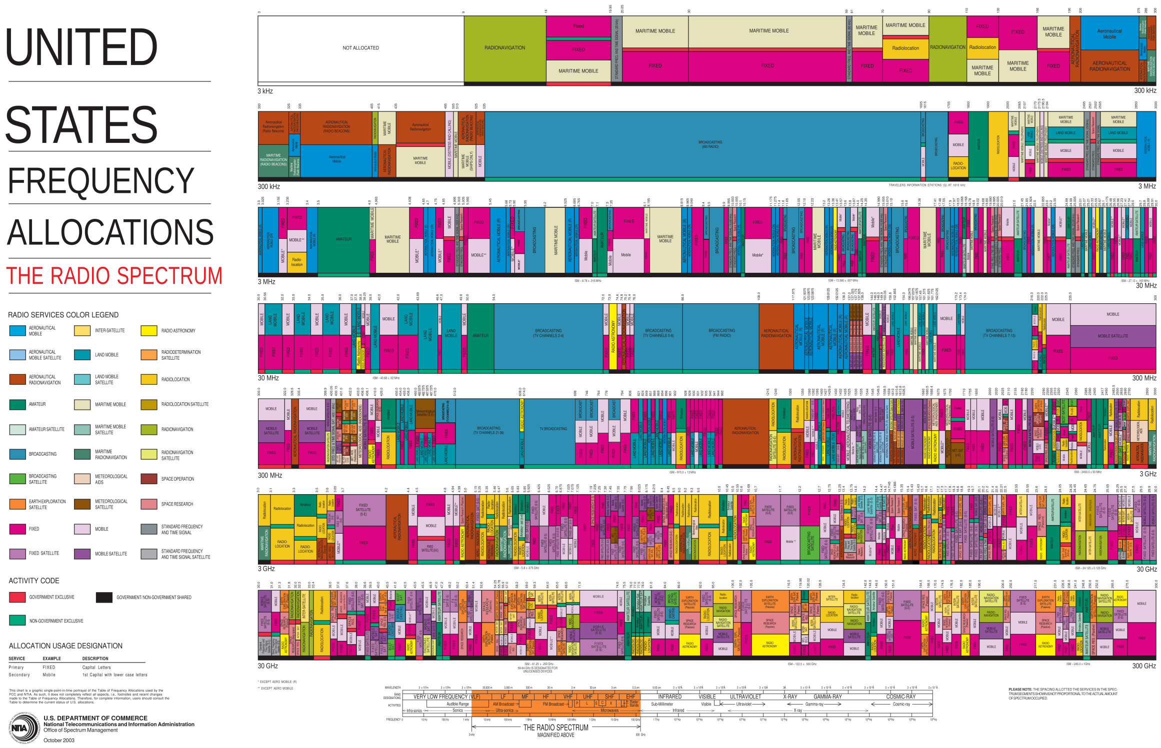

Figure 2.4: Federal Communications Commission (FCC) spectrum allocation chart [1].

Cognitive radio is a promising technology that can solve the spectrum shortage problem arising due to the rapid increase in wireless networks and mobile devices. Recent advancements in software-defined radio technology and edge computing have enhanced the cognitive radio network (CRN) capabilities and, along with some adjustments in its operation, will be a key technology for LTE-R heterogeneous network deployment. Cognitive Radio using software defined radio technology is considered to be one of the key technologies for improving the utilization of congested radio spectrum [32]. Integrating CR technology into LTE-R system is motivated by the fact that a large portion of the radio spectrum is underutilized most of the time [33]. For achieving data rates on order of gigabits per second, we need to make efficient use of available spectrum, which can be achieved by using cognitive radio network (CRNs). In CRNs, a secondary system can share spectrum bands with the incumbent primary system, either on an interference-free basis or on an interference-tolerant basis. The CR network should be aware of the surrounding radio environment and regulate its transmission accordingly. In interference-free CRNs, CR users are allowed to borrow spectrum resources only when licensed users do not use them. A key to enabling interference-free CR networks is figuring out how to detect the spectrum holes (white spaces) that are located across the spectrum and facilitates dynamic spectrum access (DSA) [34].

CR receivers should first monitor and allocate the unused spectrum via spectrum sensing (energy detection (ED), covariance absolute value (CAV) detection, etc.) [34] or combining with geolocation databases and feed this information back to the central CR controller. A coordinating mechanism is required in multiple CRNs where they all try to access the same spectrum in order to prevent users colliding with each other when accessing the same spectrum holes. In interference-tolerant CRNs, CR users can share the spectrum resource with a licensed system while keeping the interference below a threshold. In comparison with interference-free CRNs, interference-tolerant CRNs can achieve enhanced spectrum utilization by opportunistically sharing the radio spectrum resources with licensed users, as well as better spectral and energy efficiency. However, it has been shown that the performance of CR systems can be very sensitive to any slight change in user densities, interference threshold, and transmission behaviors of the licensed system [35]. However, the spectral efficiency can be improved by either relaxing the interference threshold of the primary system or considering only the CR users who have short distances to the secondary BS (utilizing the spatial gain). Hybrid CR networks have been proposed in [36] for adoption in cellular networks in order to explore additional bands and expand the capacity. CR networks can only prove beneficial if the spectrum policies related to LTE-R are implemented in a robust manner.

2.5 Train-to-train (T2T) Railway Communication

The development of driverless cars has posed some rigorous requirements for the safety of passengers and pedestrians. For safety-critical applications, transmission delays need to be less than 10 ms, which is required for intelligent transportation systems (ITSs) and vehicular networks [37]. While the road domain is being well investigated and first standards are being defined for smart vehicles (ITS-G5) standards, railway communications have mainly focused on train-to-ground (T2G) communication using GSM-R and LTE-R. There are still several challenges involved in train-to-train (T2T) communication for frequencies above 1 GHz and high speed (up to 500 Km/h) which can lead to severe fading. In [38], a measurement campaign was performed focusing on wagon-to-wagon measurements (intra-consist) with one high speed train (HST), and T2T measurements with two HSTs. A survey of channel measurements and models are presented in [39]. Various simulation and experiment results revealed that there is a trade-off between the proposed performance metrics and system parameters, such as base station (BS) and vehicle densities, radio coverage, and the maximum number of hops in a path. When LTE communication technologies have been integrated into vehicular networks, the interference has cut down the performance of LTE vehicular networks. When vehicle density is high, the beaconing signals of vehicular safety applications may easily overload the serving eNodeB. To handle this issue, a significant amount of such signals should be distributed directly among vehicles, without going through the eNB. In LTE-Advanced (LTE-A), device-to-device (D2D) communications is considered to allow direct message delivery between terminals in proximity to each other in order to lighten the load of the eNB [40].

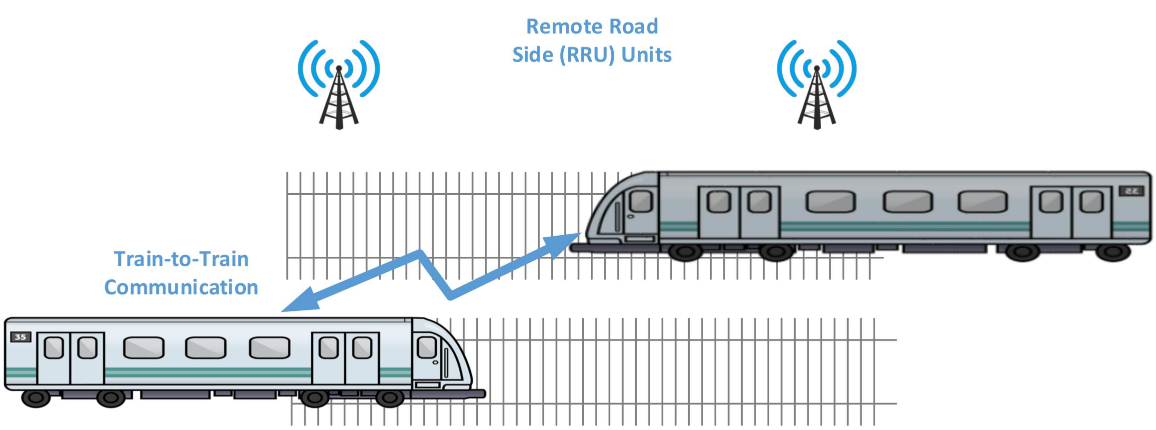

Figure 2.5: Vehicular communication using D2D 5G cellular communication technology.

The infrastructure-aided D2D technologies can serve as a natural approach to enable reliable and efficient T2T communications without negatively affecting existing cellular systems. To meet the expected performance requirements, such as low transmission delay and high throughput, a new architecture for LTE-R vehicular communication is required. Figure 2.5 describes the railway communication using D2D communication strategy where significant amount of the computation is offloaded from remote road side units (RRU) to trains in order to increase spectral efficiency. The communication environment in T2T is quite different than in D2D due to high mobility (Doppler shift) of the high speed trains. Network connectivity plays a important role in T2T communication than D2D when comparing system throughput. These features can significantly affect D2D resource allocation strategies and system parameters, and thus should be modified for railway communication.

2.6 LTE-R Services

LTE-R provides services to improve security, quality of service (QoS), and efficiency for high speed railways. Figure 2.6 shows how these services provided in LTE-R can be integrated together for a robust smart railway communication system. Some of the key services required are summarized below:

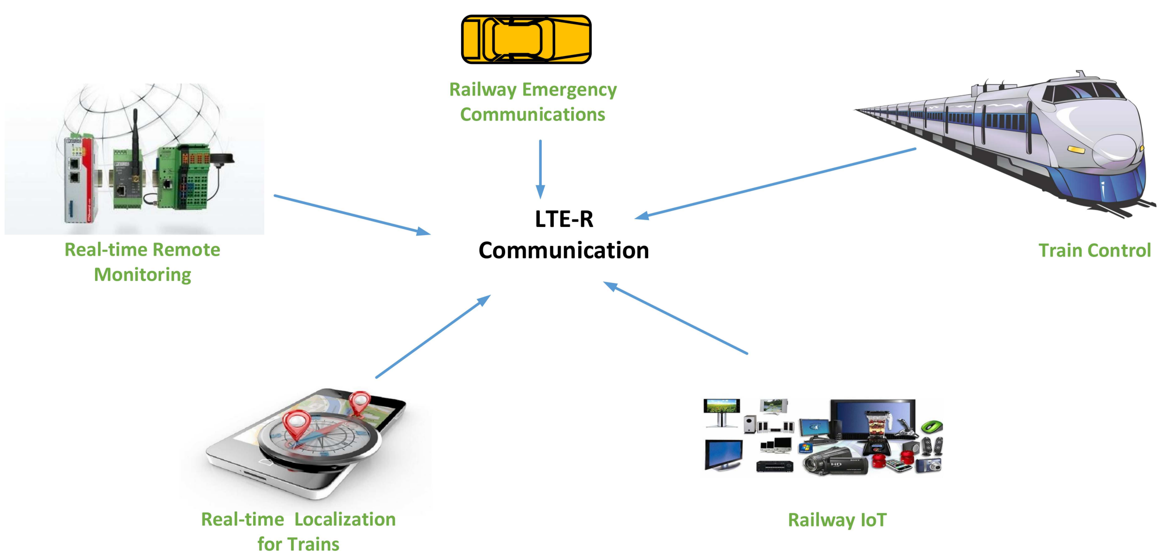

Figure 2.6: Key LTE-R services required to augment railway security, QoS and efficiency

- *Train Control*: Train control (TC) continually monitors trains, exchanging information with Train Management Computers (TMC), and gathers precise speed and position information. TC will have a copy of train orders, number of cars, weight, route and track characteristics along the route, including speed restrictions, curves, grades and crossings. Track authority, *i.e.* permission to occupy and move on a sector of track, is continuously updated as train control computers issue or modify train orders.

- *Real-time monitoring*: LTE-R should provide video monitoring of railway track conditions (flaw detection and temperature), as well as railway infrastructure to avoid accidents. The information should be transmitted in real-time with both central controller and HST with minimum delay possible.

- *Railway Emergency Communications*: Whenever there is any natural calamity or an emergency situation, an establishment of immediate communications between accident site and rescue center is of utmost importance. Railway emergency communications systems use railway private network to ensure rapid deployment and faster response compared to the existing technologies like GSM-R.

- *Real-time Localization for Trains*: LTE-R should be able to relay the real-time localization information to the central controller so that efficiency of train running can be improved. With accurate localization information train collisions can be avoided and better overall service can be provided to the passengers.

- *Railway IoT*: With railway Internet-of-Things (IoT), LTE-R can provide services such as real-time query and tracking of trains and good. It helps to improve the transport efficiency and extend service range. Railway IoT can also help in augmenting the railway safety features.

2.7 Leaky Coaxial Cable for LTE-R

Leaky Coaxial Cable (LCX) [41] is an antenna technology designed to deliver radio services in tunnel environment. It consists of small periodic slots to allow radio frequency (RF) signals to escape, which act as extended antenna elements. LCX cables were invented to provide the uniform signal coverage in underground mines where radio coverage can potentially be very limited due to the mine environment. Recently, leaky coaxial cables have been widely used in the field of railway communication, especially in tunnels. Leaky feeders are constructed from coaxial cable, where the outer shield has a series of holes with different shapes and different distances among them. The coaxial cable is usually about hundreds of metres long and can be fixed through a building or a tunnel offering radio radiation in a way that would require many individual omni-directional antennas. So far,they have been only used to supplement the direct wireless communication system between a BS and trains, mostly transmitting voice signals. Nowadays, they are being used as an alternative solution to distributed antenna systems in indoor environments such as commercial buildings [42, 43] and university buildings, high speed trains, and cars. The LCX radio system is almost noise free and has enough bandwidth to support multiple RF signals carrying voice and data simultaneously. Figure 2.7 shows the conventional leaky coaxial cable along x-axis with periodic radiating slots and wave propagation along z-axis. Generally, it consists of three parts: Inner conductor, Dielectric material, and inner conductor. LCX has a dual functionality *i.e.*, they can transmit and receive RF signals using their slots. The frequency range for a leaky cable is given by [44]:

$$\frac{c}{\sqrt{\varepsilon_r - 1)d}} \geq f \leq \frac{c}{\sqrt{\varepsilon_r} + 1)d}. \tag{2.1}$$

where c is the speed of light in m/s, d is the length of the LCX cable and ε_r is the relative permittivity of the tunnel walls.

A radio system based on LCX has been deployed in Japan for high speed railways "Series N700" [45] to connect the train to ground network. Wi-Fi access points are chosen for in-train communications with peak data rates of 2 Mbps for uplink and downlink. Although current technologies can provide wireless communication services in HSTs, the capacity of communication system is very low (1–4 Mbps). These data rates are insufficient for next generation wireless communication system where the peak data rates of 0.5 – 5 Gbps are expected. LTE-R communication system can be implemented for achieving high data rates but it cannot be achieved by using conventional cellular systems. The penetration loss due to the tunnel walls is very high and secondly, the fast moving trains cause large

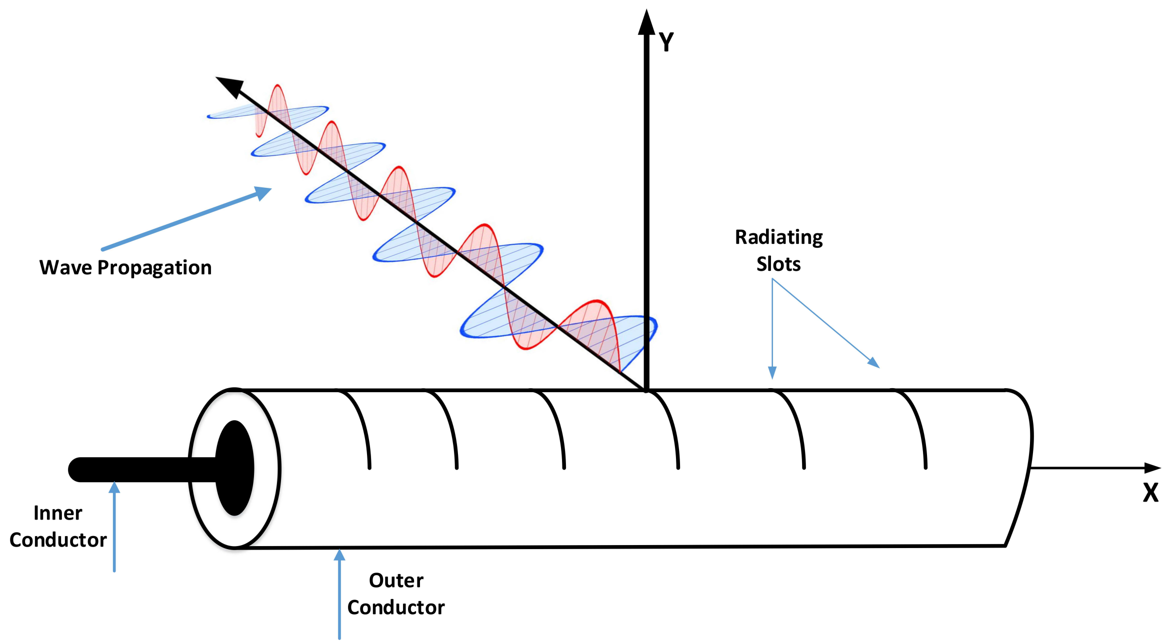

Figure 2.7: Leaky Coaxial Cable used for uniform radio coverage in a Tunnel environment. [2]

Doppler shifts leading to poor connectivity due to retransmissions. Hence, leaky coaxial cable is potentially the best candidate for achieving extensive internet access inside a tunnel environment for high speed railways.

2.8 Summary

This chapter outlined and examined the topics of positive train control, WiBro, LTE-R communication system and provided a foundation for smart railway communication system. We also discuss the spectrum regulation for LTE-R, T2T railway communication, various services required in LTE-R and finally leaky coaxial cables (LCX) for uniform coverage in a tunnel environment. Next in this thesis, we consider heterogeneous cooperative spectrum sensing (CSS) and how it can be use to augment smart railways. After CSS, we discuss the implementation and results of our proposed test-bed for high speed train and software-defined radios.

Chapter 3

Heterogeneous Cooperative Spectrum Sensing (CSS)

This chapter provides the background information needed to understand and implement cooperative spectrum sensing. It examines the basic outlines of a heterogeneous networks and how cooperative spectrum sensing (CSS) can help in enhancing the accuracy of signal source estimation. The fusion center (FC) collects the data from the sensor node network and processes it to make a reliable decision. Second, this chapter investigates various algorithms that can be used in heterogeneous network to estimate signal source. Finally, the necessary hardware and software tools used in the implementation of heterogeneous CSS prototypes is provided.

3.1 Spectrum Sensing

Spectrum sensing plays a key role in the decision-making part of cognitive radio networks. It is required by CR to detect the presence of spectrum white spaces and also to accurately estimate the presence of incumbent users (PUs). Since the PUs have the prerogative on the spectrum band usage, so it is of paramount importance to avoid interfering with the PU when performing dynamic spectrum access. It is very challenging to get an accurate estimate under a practical fading environment based on conventional spectrum sensing techniques. Various non-idealities such as shadowing, multipath, and fluctuating noise variance can make it difficult to detect the primary user. In the case of fast varying channels over time, several works focus on improving the performance of the spectrum sensing and signal identification [46–48]. To combat the Doppler shift caused due to high-speed environments, algorithms [49] have been proposed for channel estimation and equalization. Cooperative spectrum sensing [50] can be use to address many of these problems caused due to multipath, shadowing, and high Doppler shift. In the thesis, we evaluated the performance of cooperative spectrum sensing using soft and hard data fusion schemes via software-defined radio prototype hardware. The experiment confirmed that cooperation among sensor nodes will improve the spectrum sensing performance as a result of increased spatial-temporal diversity of the received signal source. The various types of spectrum sensing schemes are discussed below in the following subsections.

3.1.1 Energy Detection

In energy detection (ED) we use the energy spectra of the received signal and compare it against a predefined threshold level to estimate the presence of the signal.In an ED scheme we only rely on the energy of the signal in the frequency channel and no phase information is required. The key advantage of the ED scheme is that it does not require any prior information of the signal, *i.e.*, type of modulation scheme, phase information or any other signal parameter. Energy detection can be considered as a binary hypothesis testing scheme and is given by [15]:

$$y(n) = \begin{cases} w(n), & \mathbf{H}_0 \\ s(n) + w(n), & \mathbf{H}_1 \end{cases} \tag{3.1}$$

where $y(n)$ represents the received signal, $s(n)$ represents the signal source (PU), and $w(n)$ is the white Gaussian noise $w(n) \sim N(0, \sigma_n^2)$. $\mathbf{H}_0$ describes the hypothesis when there is no signal present, while the hypothesis $\mathbf{H}_1$ is the presence of signal. Figure 3.1 explains the energy detection scheme in the form of a block diagram. First, the analog signal $X(t)$ is converted into digital domain via analog-to-digital (ADC) converter, then the Fast Fourier Transform (FFT) block converts the signal from time domain to frequency domain. We then calculate the magnitude square of the signal and finally we take the average over the N values to compute the decision statistic δ. The δ is compared with the threshold to estimate the presence or absence of the signal.

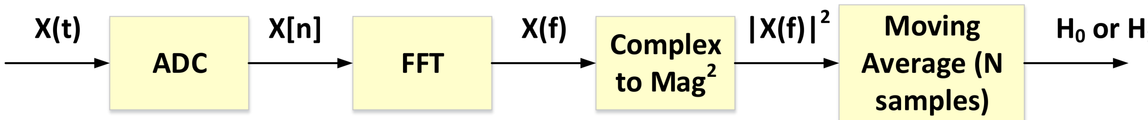

Figure 3.1: The block diagram describing the working of energy detection scheme [3].

The decision whether the signal is present or absent is decided by evaluating a local test statistic L to see whether it is above or below certain fixed threshold τ. The local test statistic L, which is the complex-magnitude squared of the FFT samples, is compared with τ using equation:

$$L = \sum_{n=1}^{M} |y(n)|^2 = \begin{cases} < \tau, & \mathbf{H}_0 \\ > \tau, & \mathbf{H}_1 \end{cases} \tag{3.2}$$

where $|y(n)|^2$ is the energy of a specific FFT bin and $n = 1, 2, 3...M$ are the number of samples received. The probability of false alarm P_{fa} and probability of detection P_d are given by [15]:

$$P_f = Q\left(\frac{\tau - M(2\sigma_n^2)}{\sqrt{M}(2\sigma_n^2)}\right), \tag{3.3}$$

$$P_d = Q\left(\frac{\tau - M(2\sigma_n^2)(1+\gamma)}{\sqrt{M(1+2\gamma)}(2\sigma_n^2)}\right). \tag{3.4}$$

where M_r is the number of samples used to estimate the power of the signal source in the node, $\sigma_{n,r}$ is the noise variance and τ is the threshold.

3.1.2 Cyclostationary Method

There are several applications where it is required to perform the modulation recognition and signal classification. Communication signals can be more accurately described as statistical processes which repeats themselves cyclically or periodically rather than a stationary process. Mathematically, Cyclostationary feature detection scheme can be described by the equation [3]:

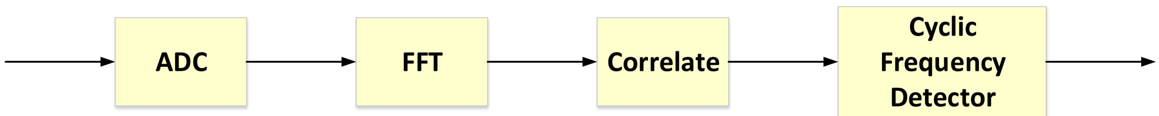

Figure 3.2: The block diagram describing the working of cyclostationary feature detection scheme.

$$R_x(t,\tau) = E\Bigg\{x\Bigg(t+\tau\Bigg)x^*\Bigg(t-\tau\Bigg)\Bigg\} = \sum_{\{\alpha\}} R_x^{\alpha}(\tau)e^{j2\pi\alpha t} \tag{3.5}$$

where R_x is the cyclic autocorrelation function, α is the fundamental cyclic frequency. The Eq.(3.5) shows the autocorrelation of the observed signal $x(t)$ with periodicity τ, $E\{.\}$ is the expectation operator, $\{\alpha\}$ is the set of Fourier components and R_x^{α} is the cyclic autocorrelation function (CAF) and is given by:

$$R_x^{\alpha} = \lim_{T\to\inf} \int_{-T/2}^{T/2} R_x(t,\tau)e^{-j2\pi\alpha t}. \tag{3.6}$$

Figure 3.2 shows the block diagram implementation of cyclostationary feature detection scheme, where we correlate the frequency domain signal and then pass it to the cyclic frequency detection block and perform the signal classification.

3.1.3 Matched Filter Detection

In the matched filter detection method, a known signal is correlated with an unknown signal captured from the available radio resource to detect the presence of pattern in the unknown signal. It is an optimal filter that projects the received signal in the direction of the pilot signal x_p(n) [51]. The test statistic is given by:

$$T_{MD} = \sum_{N} y(n)x_p^*(n). \tag{3.7}$$

where $y(n)$ is the received signal. The test statistic T_{MD} is compared with a particular threshold to decide whether the signal is present or absent.The probability of detection P_d

and probability of false alarm P_{fa} can be expressed as:

$$P_d = Q\left(\frac{\lambda - E}{\sqrt{E\sigma_{n,r}^2}}\right), \tag{3.8}$$

$$P_{fa} = Q\left(\frac{\lambda}{\sqrt{E\sigma_{n,r}^2}}\right). \tag{3.9}$$

where E is the energy of the signal source, λ is the detection threshold, and $\sigma_{n,r}$ is the noise variance. The use of matched filter is very limited due to the requirement of *a priori* information which is not feasible in most cases.

3.2 Cognitive Radios

Cognitive Radio (CR) [52] is a communication systems paradigm that focuses on employing highly agile, environmentally aware, intelligent wireless platforms in order to autonomously select and configure device operating parameters based on the prevailing radio and network environmental conditions [3]. In general, cognitive radio may be expected to look at parameters, such as channel occupancy rate, available channels, bandwidth required for data transmission, and the modulation types that may be used. It must also look at the regulatory requirements set by the Federal Communications Commission (FCC). In some instances, a knowledge of geography and this may alter what we are permitted to do. Software-defined radios (SDRs) are mainly responsible for making cognitive radios used in wireless communications system a reality. Software radios provide the potential to personalize services, and they make the process of modifying the radio characteristics simpler.

To facilitate the intelligent decision making capabilities in these cognitive radio systems, machine learning algorithms have been proposed in the literature [35, 53–55] to automate the reconfiguration process. Figure 3.3 describes the various building blocks of a cognitive radio system. The spectrum sensing is performed to estimate the spectrum holes in the band and after the analysis the decision strategy is prepared. The radio is configured with the new parameters based on the radio environment and the spectrum decision made.

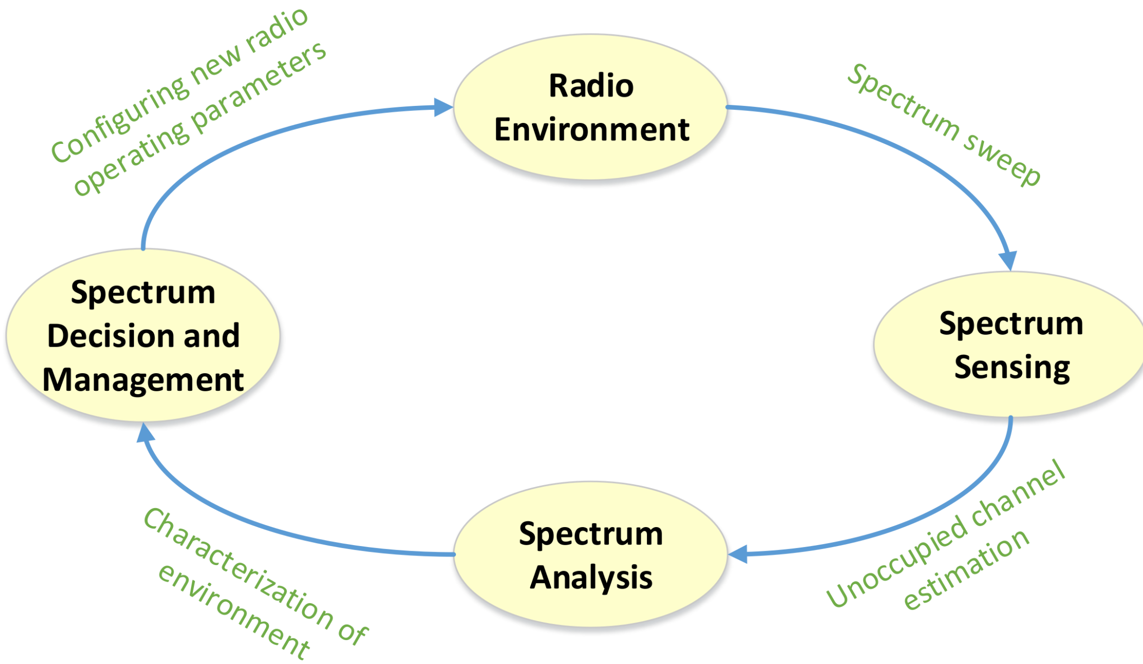

Figure 3.3: The block diagram explaining the basic parts of Cognitive Radio system. The operating parameters are configured based on the characterization of the wireless environment.

3.3 CSS in Heterogeneous Networks

In Heterogeneous CRNs, each radio is equipped with different numbers of antennas, sampling rates and RF characteristics. Additionally, each sensor node may experience distinct channel fading and suffer from different noise levels due to their respective locations and device performances, such as amplifiers and ADCs. As a result, each node may have different sensing capabilities and reliability values. This is a universal and fundamental characteristic of a heterogeneous CRN, which requires robust algorithms to achieve high accuracy in signal source detection for estimating the presence of a primary user [56]. In this thesis, we investigate the cooperative spectrum sensing in heterogeneous networks with a centralized FC, a transmitter acting as a signal source, and four sensor nodes. As explained earlier, we are using energy detection as one of the spectrum sensing technique since it possesses a very low implementation complexity [15]. The energy detection scheme detects the presence or absence of a signal source based on its intercepted energy signature.

If the energy of the signal is higher than a certain threshold, this indicates that the channel is occupied.

In cooperative spectrum sensing, each sensor node transmits the local sensing data to the fusion center for signal source detection. The local sensing data has to be quantized, thus yielding quantization errors. To minimize the quantization error in local test statistic L and to reduce the effect of noise variance, the energy of the received signal $y(n)$ is normalized [56]. The local test statistic L for the r^{th} sensor node is given as:

$$L_r = \frac{1}{M_r \sigma_{n,r}^2} \sum_{r=1}^{M_r} |y(n)|^2 \tag{3.10}$$

where M_r is the number of samples used to estimate the power of the signal source in the node, $\sigma_{n,r}$ is the noise power variance.

In Eq.(3.1), $s(n)$ is considered to be a deterministic signal and $w(n)$ is a Gaussian random variable with a variance of σ_n^2. Based on CLT, L_r will have a following distribution [18]:

$$L_r = \begin{cases} N(1, \frac{1}{M_r}), & \mathbf{H}_0 \\ N(\gamma_r + 1, \frac{1 + 2\gamma_r}{M_r}), & \mathbf{H}_1 \end{cases} \tag{3.11}$$

where γ_r is the received SNR of the r^{th} SU. The local decision statistic L_r is quantized before transmission due to the bandwidth constraint, and this can lead to quantization errors. The values of L_r received by FC can be modeled as:

$$\beta_r = L_r + w_{q,r}, \tag{3.12}$$

where β_r is the decision statistic received by the FC and w_q is the noise added to the signal due to fading and quantization error. In [57], the w_q is modeled as a Gaussian noise with zero mean and σ_q^2 variance.

3.4 Software Defined Radios

We have already explained about the cooperative spectrum sensing in heterogeneous networks, now in this section we will look at the platform for testing the CSS algorithms.

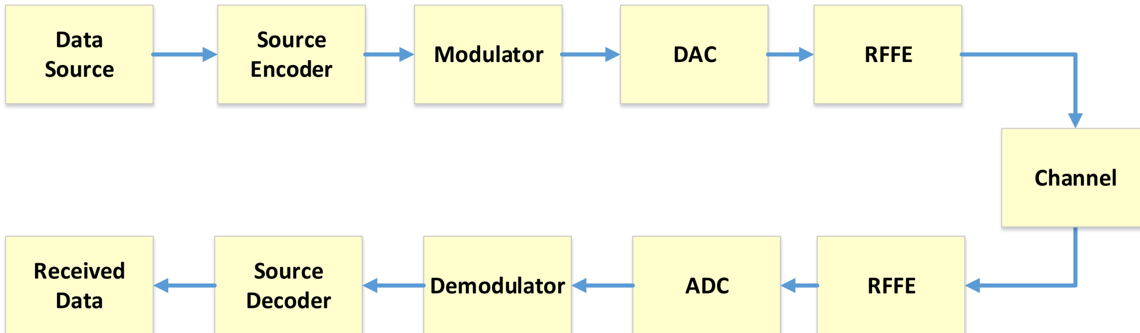

Figure 3.4: Software defined radio pushes all the adaptive elements and data manipulation operation into software. The goal of SDR is to provide or define all of the radio operation in software.

The platform which we use is a new hardware frontier called Software-Defined Radio (SDR) and is discussed in details.

There has been a huge shift in the definition of a Software-Defined Radio and it has much to do with the question of where the hardware ends and the software begins. Mitola coined the term Software Defined Radio, which he described as a of digital signal processing (DSP) primitives, a meta-level system for combining the primitives into communication system (Tx, channel model, Rx, etc.), functions, and a set of target processors on which the software radio is hosted for real-time communications [58]. Mitola explains in his thesis how software provides the flexibility which using hardware alone can never be achieved.

SDR technology existed since the 1970s [3] but the key milestone in the advancement of SDR technology took place in early 1990s with the U.S. military initiative called SpeakEasy I/II. The SpeakEasy project was implemented to use programmable processing in order to emulate more than ten existing military radios, operating in frequency bands between 2 MHz and 2 GHz [59]. With SpeakEasy, the operator could talk to ten radios operating under different standards with any hardware modifications. With all of these features, unfortunately, there were some shortcomings which left much to be desired. The device was large enough to fit on the back of a pickup truck [59], which is good for ground station but not if the mobility is an important factor. In 1992 the field programmable gate arrays (FPGA) were not computationally efficient, hence required a large amount of time to change their operating characteristics.

The two software-defined radios we used in the thesis are Universal Software Radio Peripheral (USRP N210) and RTL-SDR R2832U. In the subsequent subsections, we discuss the two SDRs in detail.

3.4.1 USRP N210 and RTL-SDR

The USRP N210 and RTL-SDR are two very different SDR platforms when compared with each other, as shown in table 3.5. The USRP N210 provides a very high bandwidth, dynamic range processing capability. The product architecture includes a Xilinx Spartan 3A-DSP 3400 FPGA [60], 100 MS/s dual ADC, 400 MS/s dual DAC, and gigabit ethernet connectivity to stream data to and from host processors. A modular design allows the USRP N210 to operate from DC to 6 GHz, while an expansion port allows multiple USRP N210 series devices to be synchronized and used in a MIMO configuration. An optional GPSDO module can also be used to discipline the USRP N210 reference clock to within 0.01 ppm of the worldwide GPS standard. The USRP N210 can stream up to 50 MS/s to and from host applications. Users can implement custom functions in the FPGA fabric, or in the on-board 32-bit RISC softcore. The USRP N210 provides a larger FPGA than the USRP N200 for applications demanding additional logic, memory and DSP resources. The FPGA also offers the potential to process up to 100 MS/s in both the transmit and receive directions. The FPGA firmware can be reloaded through the Gigabit Ethernet interface [27].

Table 3.1: Comparing different technical specifications of USRP N210 and RTL-SDR

Specifications	USRP N210	RTL-SDR
Maximum Sampling Rate	100 Msps	3.2 Msps
ADC Resolution	14 bits	8 bits
Frequency Range	400 MHz–4.4 GHz	24 MHz–1766 MHz

RTL-SDR is a very cheap software defined radio that uses a DVB-T TV tuner dongle based on the RTL2832U chipset. With the combined efforts of Antti Palosaari, Eric Fry, and Osmocom, it was found that the signal I/Q data could be accessed directly, which

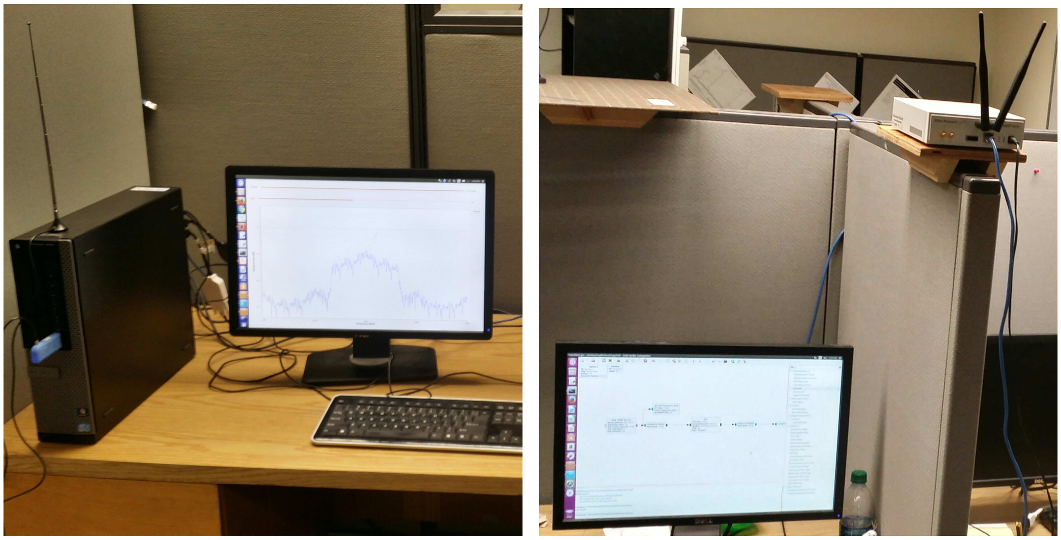

(a) RTL-SDR (b) USRP N210

Figure 3.5: RTL-SDR and USRP running a GNU Radio flow-graph and performing spectrum sensing at 450 MHz using normalized energy detection.

allowed the DVB-T TV tuner to be converted into a wideband software defined radio via a new software driver. Essentially, this means that a cheap $20 TV tuner USB dongle with the RTL2832U chip can be used as a computer based radio scanner. This sort of scanner capability would have cost hundreds or even thousands of dollars just a few years ago. The RTL-SDR is also often referred to as RTL2832U, DVB-T SDR, RTL dongle or the $20 Software Defined Radio. Figure 3.5 shows the RTL-SDR and USRP N210 running a GNU Radio flowgraph and performing spectrum sensing.

3.4.2 GNU Radio and MATLAB

We have used GNU Radio [61] and MATLAB [62] software in the thesis to implement the cooperative spectrum sensing for hard decision and soft decision schemes. GNU Radio is an open source development toolkit that provides reconfigurable signal processing blocks to implement and test out software-defined radios and signal processing systems. GNU Radio allows for SDR developers to develop unique signal processing blocks and SDR systems. GNU Radio was started in 2001, originally forked from the SpectrumWare project developed at the Massachusetts Institute of Technology [63]. Since 2001, the code base has undergone massive changes, containing almost no code from the original SpectrumWare project [64]. Physically the code consist of three languages Python, C++, and SWIG. Python provides the overarching control of the system or program, while C++ provides the actual signal processing blocks and mathematics. SWIG is a wrapper for C++ which allows Python to dynamically wrap around C++ and control or compile with it. Figure 3.6 better illustrates this architecture. It is also important to mention that there are significant paradigm shifts in the community, pushing more and more code to Python rather than C++, due to its easier programming syntax and structure [65]. In Figure 3.7 we implemented a simple energy detection scheme by using available signal processing blocks in GNU Radio.

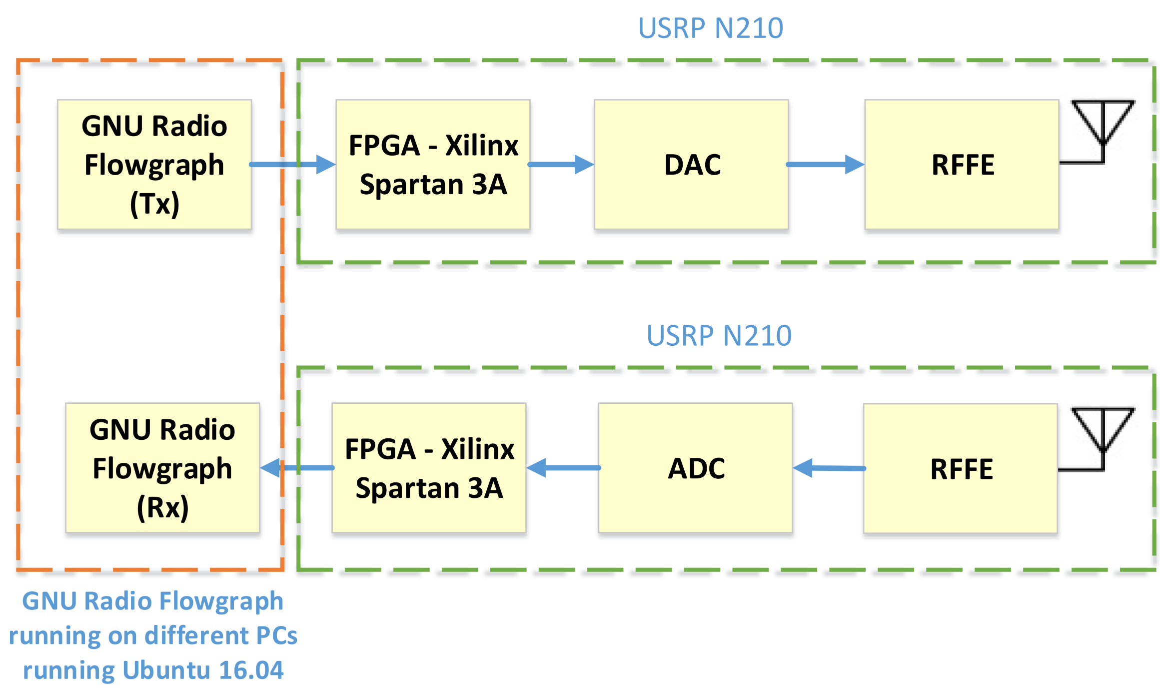

Figure 3.6: Block diagram describing the flow of information between GNU Radio and USRP N210. USRP N210 has in-built Xilinx Spartan 3A FPGA for designing reconfigurable SDR test-beds.

The GNU Radio software provides the framework and tools to build and run software radio or just perform general signal processing applications. The GNU Radio applications themselves are generally known as ”flow-graphs”, which are a series of signal processing

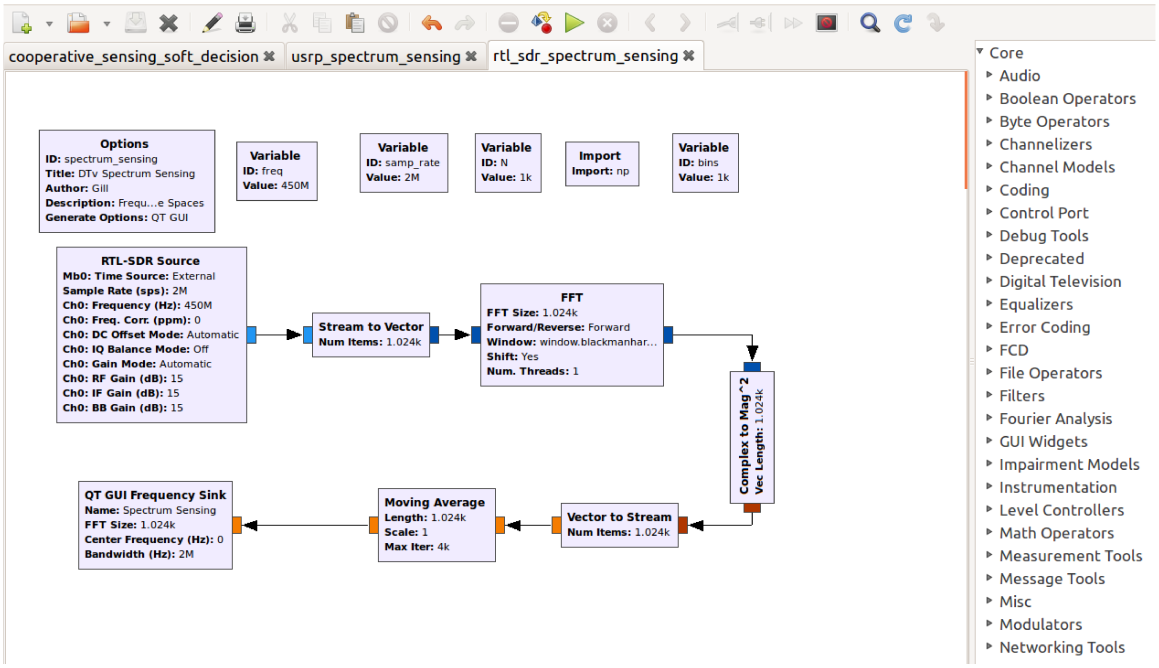

Figure 3.7: GNU Radio flow-graph for spectrum sensing using energy detection using RTL-SDR source.

blocks connected together, thus describing a data flow. GNU Radio provides a very structured framework of flow design. Data processing segments are highly self contained in order to minimize error propagation during system debugging. Since the software is open-source, full access to all code is provide, giving low-level access to all operations within GNU Radio. Much of the actions have been abstracted to the limited knowledge of the lower layers, but if specific actions are required for an application then serious depth or knowledge is needed about the overall projects structure.

MATLAB is an extremely well known engineering, mathematical, biological, and financial software suite. MATLAB provide massive data leverage and advanced communication system models and algorithm for significant data processing. In this thesis, we have used MATLAB for post-processing, where the results are later used in MATLAB which acts as a FC, and makes the decision based on the global test statistic for both hard and soft data fusion mechanism. Spectrum sensing data collected by the sensor nodes is dumped into static files, which are later processed in MATLAB to make decisions. Figure 3.8 shows the

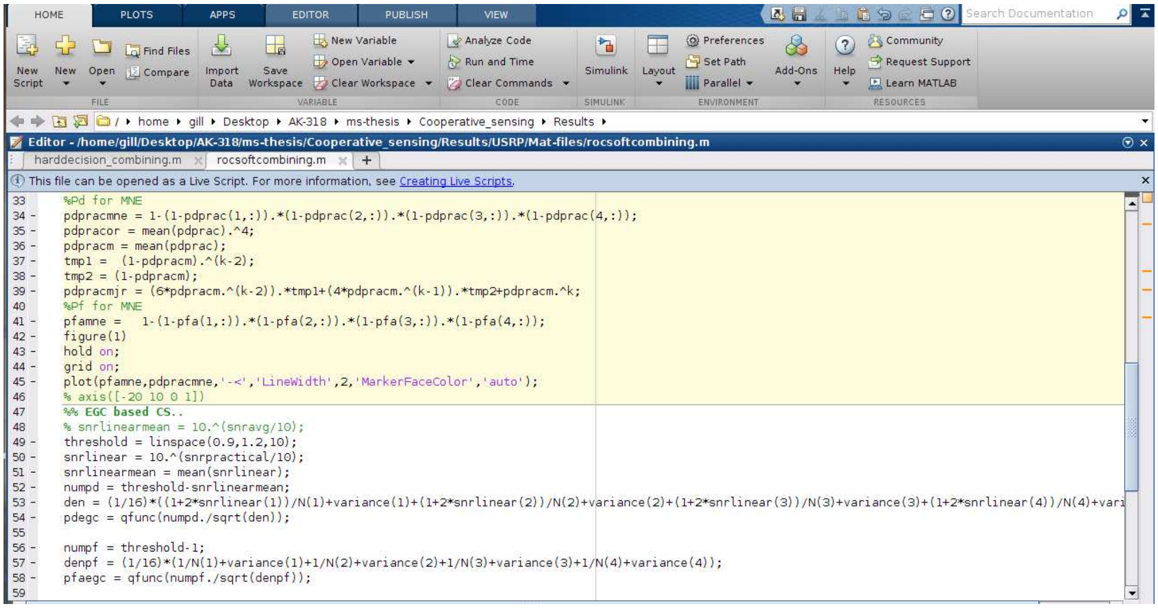

Figure 3.8: Screen capture of MATLAB editor running a code for computing receiver operating characteristics of soft decision combining scheme.

MATLAB editor where we computing the ROC characteristics of soft and hard decision combining schemes. The plots are also generated to compare both the schemes by data files collected in GNU Radio.

3.5 Summary

In this chapter, we discussed the heterogeneous cooperative spectrum sensing and examined various spectrum sensing techniques. We also discussed cognitive radios, CSS in heterogeneous networks, and software-defined radios in details. We discussed three popular spectrum sensing techniques and also describe the software-defined radios USRP N210 and RTL-SDR as well as their RF characteristics. Finally, we described the GNU Radio and MATLAB software tools used in the thesis to implement the proposed CSS test-bed.

Chapter 4

Proposed LTE-R Channel Model and Framework

This chapter provides background information on proposed LTE high-speed railway communication system. It outlines the architecture for LTE-R leveraging the existing LTE network for high speed railway networks. For uniform coverage inside a tunnel environment, leaky coaxial cables (LCX) have been proposed for efficient communication. The severe channel impairments inside a tunnel are also discussed with special attention given to high Doppler shift caused by the high velocities of trains and harsh multipath fading environment. The proposed two-ray propagation channel model is discussed and mathematical derivations of the K-factor is described. We then discuss our LTE-R test-bed implementation in MATLAB and compare the performance for QPSK, 16QAM and 64QAM modulation schemes in a tunnel environment. First, we show the results of K-factor variation in a tunnel environment for a high speed train in a tunnel. Using the K-factor, we then implement our channel model, which also takes into effect the high Doppler shift due to mobility of the train. The bit-error rate curves are generated for the LTE-R modulation schemes for the proposed channel model for high speed train in a tunnel. Finally, we show a time-varying BER curve for high speed train moving with the velocity v at discrete timesteps.

4.1 Channel Impairements Inside a Tunnel

The tunnel environment is affected by multipath and diffraction effects due to multiple reflections from the tunnel walls, which leads to a substantial fading environment. By deploying LCX cables, we can eliminate the large penetration loss due to tunnel walls. However, small-scale fading can still cause a large amount of errors and decrease the QoS for the communication link. High velocity trains experience very high Doppler shifts and a fast fading channel. These problems can lead to significant BER degradation of the LTE system. The frequency shifts caused by the Doppler phenomenon can lead to shifts in the sub-carrier frequencies for OFDM, which leads to synchronization errors [21]. The maximum Doppler shifts for a train traveling at 500 km/h is 2.314 kHz for a 5 GHz carrier frequency. This large Doppler shift can also lead to significant drops in the quality of wireless signals and increase the bit error rate. Thus, to develop an efficient and reliable communication link inside tunnels, we need to properly model this channel impairment and build our proposed channel model by taking into account these tunnel phenomena. These impairments are described in detail in the following subsections.

4.1.1 Multipath Fading

The following time-varying multipath channel impulse response considers the effects of Doppler shift and scattering [66]:

$$h(\tau, t) = \sum_{k=0}^{L} h_k(t) e^{-j2\pi f_c \tau_k(t)} \delta[\tau - \tau_k(t)], \tag{4.1}$$

where τ is the path delay, t is time in seconds, $\delta[\tau - \tau_k(t)]$ is the impulse response, f_c is the carrier frequency, $h_k(t)$ is the envelope of the time-varying channel and consists of both large and small-scale fading components. Since the structure of LCX is almost the same as a leaky waveguide, the large scale fading of channel can be modeled linearly [2]. There is also no signal shadowing and the line-of-sight (LOS) signal component is always present along the tunnel. This type of channel fading can be best described by a Ricean fading model. The probability density function $p(\alpha)$ of a Rician fading model is given by [67]:

$$p(\alpha) = \frac{2\alpha(1+K)}{\Omega} I_0\left(2\alpha\sqrt{\frac{K+K^2}{\Omega}}\right) e^{\frac{-K-\alpha^2(1+K)}{\Omega}}, \tag{4.2}$$

where K is the Rician factor and α is the complex amplitude of the channel response function that has a unity second moment, *i.e.*, $\Omega \equiv E[\alpha^2] = 1$.

4.1.2 Doppler Shift

The 3GPP channel model [68] is used for its Doppler shift profile in high speed railway environment. The measurements obtained for the Doppler frequency shift are implemented for two scenarios. The first scenario is for an open space while the second scenario is for high speed trains. Doppler shift is not taken into consideration. There exists a third scenario for tunnels using multiple antennas. Since the slots of the LCX can be modeled as multiple antenna system, we use this Doppler shift profile for our proposed channel. The Doppler shift variation $f_s(t)$ is described by:

$$f_s(t) = f_d \cos\theta(t), \tag{4.3}$$

where f_d is the maximum Doppler shift, θ is the elevation angle and $\cos\theta(t)$ is given by:

$$\cos\theta(t) = \begin{cases} \dfrac{D_s/2 - vt}{\sqrt{\mathrm{D_{min}}^2 + \left((D_s/2) - vt\right)^2}}, 0 \le t \le \dfrac{D_s}{v} \\ \dfrac{-1.5D_s + vt}{\sqrt{\mathrm{D_{min}}^2 + \left((-1.5D_s) - vt\right)^2}}, \dfrac{D_s}{v} \le t \le \dfrac{2D_s}{v} \end{cases} \tag{4.4}$$

where $D_s/2$ is the initial distance of the train from base-station, and D_{min} is base-station (BS)-Railway track distance, both in meters, v is the velocity of the train in m/s, and t is time in seconds.

Figure 4.1 shows the Doppler spectrum for $f_c = 5$ GHz and $v = 300$ Km/h, 400 Km/h and 500 Km/h, and as we can see in the figure the maximum Doppler shift range is from -2.314 kHz to +2.314 kHz. These ranges of Doppler shift values can lead to very high bit-error rate and poor connectivity in communication system. In the following section,

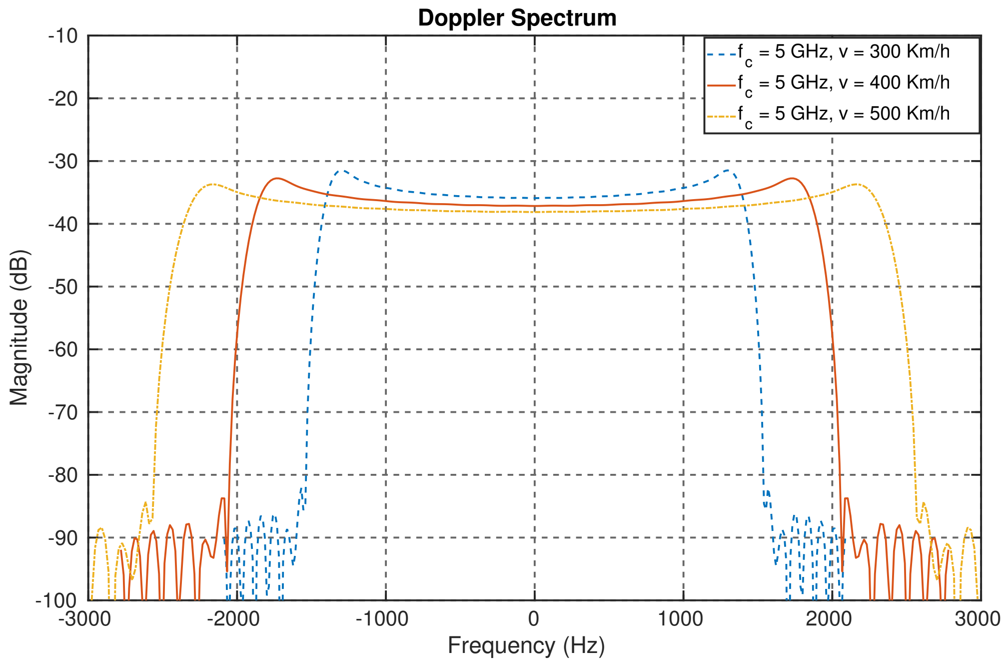

Figure 4.1: Doppler spectrum for LTE-R at different train velocities v (km/h) $=$ 300, 400 and 500 and $f_c = 5$ GHz.

we discuss our proposed channel model that consists of Doppler shift profile for high speed train and dynamic K-factor for tunnel environment.

4.2 Proposed Channel Model

The tunnel measurement campaign conducted in [20] shows that the amplitude variation inside tunnel follows Rician distribution. In the thesis, we apply the approach used in [69] for single elevation angle θ and expand it to a time-varying case. In this thesis, we model θ as a function of time and derive time-series K-factor for the tunnel environment. Figure 4.2 describes our proposed channel model which is implemented using dynamic K-factor and Doppler shift profile derived using Eq. (4.3). In the following section, we discuss the classical two-ray propagation model and mathematical derivation of dynamic K-factor for our proposed channel model.

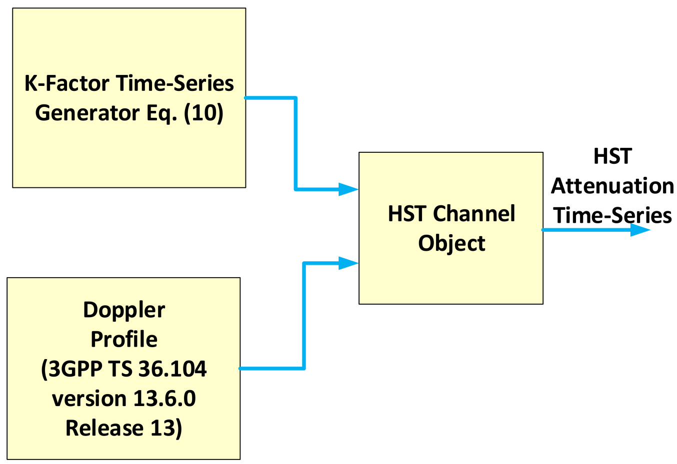

Figure 4.2: HST channel model consisting of time-series K-factor and Doppler shift caused due to velocity of the train.

The reflection coefficient Γ [70] as a function of time t is given by:

$$\Gamma(t) = \frac{C\sin\theta(t) - \sqrt{(\varepsilon_r - j\chi(t)) - (\cos\theta(t))^2}}{C\sin\theta(t) - \sqrt{(\varepsilon_r - j\chi(t)) - (\cos\theta(t))^2}}, \tag{4.5}$$

where $C = 1$ is for horizontal polarization, and $C = \varepsilon_r - j\chi(t)$ for vertical polarization. Furthermore, $\chi(t)$ is given by:

$$\chi(t) = \frac{\sigma}{\omega(t)\varepsilon_0} = \frac{\sigma}{2\pi f_r(t)\varepsilon_0} = \frac{1.8\times 10^{10}\sigma}{f_r(t)}. \tag{4.6}$$

with $\varepsilon_0 = 8.854\times 10^{-12}$ F/m, and σ is conductivity of the tunnel. The frequency $f_r(t)$ is the resultant frequency caused by the Doppler shift and is given by:

$$f_r(t) = f_c(t) - f_s(t) \tag{4.7}$$

where $f_c(t)$ is the sub-carrier frequency, and $f_s(t)$ is the Doppler shift given by Eq. (4.3).

The phase difference function of t, $\Delta\phi(t)$, between the two reflected paths is given by [26]:

$$\begin{aligned}\Delta\phi(t) =& \frac{2\pi}{\lambda(t)}\Bigg(\sqrt{D_{\mathrm{LOS}}^2 + (h_t + h_r)^2} - \\ & \sqrt{D_{\mathrm{LOS}}^2 + (h_t - h_r)^2}\Bigg),\end{aligned} \tag{4.8}$$

where $\lambda(t)$ is the resultant time-varying wavelength at the receiver, D_{LOS} is the distance between the transmitter and receiver antennas which is changing dynamically with t, and both h_t and h_r are the heights of the transmitter and receiver antennas, respectively.

Table 4.1: Tunnel and Tx/Rx Characteristics

	Dimensions	Simulation Parameters
Tunnel	Width = 8.6 m, Height = 7.3 m	$\varepsilon_r = 5$, $\sigma = 0.1$ Sm^{-1}
Leaky Feeder Cable (Tx)	Height = 6.1 m	f_c (GHz) = 2, 3, 5
Train (Rx)	Height = 4.2 m	v (km/h) = 300, 400, 500

The resultant received power $p_r(t)$ is given by the sum of the LOS received power plus the received multipath power, resulting in:

$$p_r(t) = p_t(t)\left(\frac{\lambda}{4\pi d}\right)^2 G_t G_r \Big[1+ |\Gamma(t)|^2 + 2|\Gamma(t)|\cos(\angle\Gamma(t) - \angle\Delta\phi(t))\Big], \tag{4.9}$$

which is a function of the transmitter power $p_t(t)$ and the reflection coefficient $\Gamma(t)$, where G_t and G_r are the transmitter and receiver antenna gains, respectively. The K-factor is defined as the ratio of the direct path power and the power in the scattered paths, and is given as:

$$\mathrm{K}(t) = \frac{1}{|\Gamma(t)|^2 + 2|\Gamma(t)|\cos(\angle\Gamma(t) - \Gamma(t)\Delta\Phi(t))} \tag{4.10}$$

4.3 LTE-R Testbed in MATLAB

We have implemented the simulation testbed in MATLAB, consisting of a transmitter, a channel and a receiver. The K-factor values for the channel model are obtained from Eq .(4.5) and are used to generate a time-series BER curve for different modulation schemes used in LTE-R. The values used for the electrical material properties for tunnel walls [71] and its specifications are given in Table 4.1. The relative permittivity for the tunnel walls is taken as $\varepsilon_r = 5$ and σ is set to 0.1. The simulation is conducted for velocity of $v = 300$, 400 and 500 Km/h. Since the frequency band allocation for LTE-R will most probably be from 2–6 GHz, hence the f_c values chose are 2, 3 and 5 GHz. The height of the receiver is assumed to be around the length of the train and height of tunnel is chosen as the size of the leaky coaxial cable.

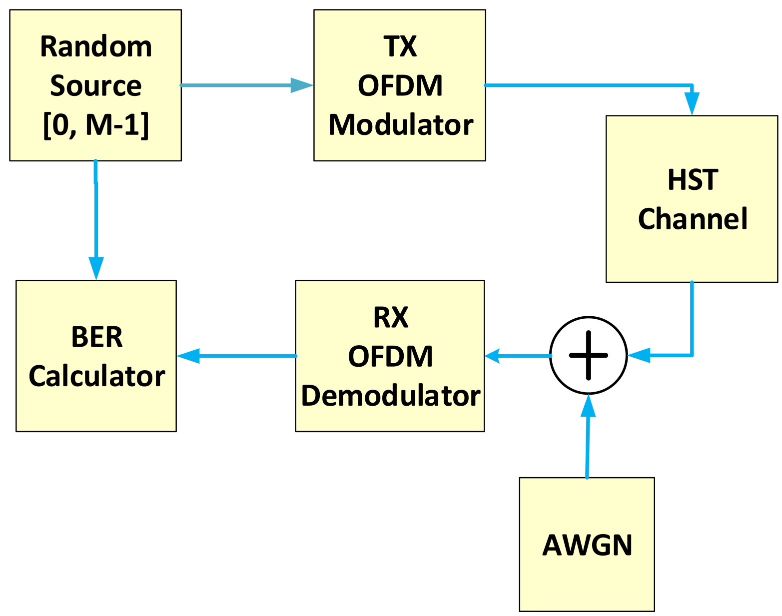

Figure 4.3: Block diagram of a communication system through a HST channel using QPSK, 16-QAM and 64-QAM.

Figure 4.3 shows the block diagram of the simulation test-bed used for the performance analysis of LTE-R. The random source block generate the symbol between 0 and $M-1$, where $M = 4, 16, 64$ for QPSK, 16QAM and 64QAM, respectively. The data is then modulated with specific modulation type and then pass through the proposed HST channel model. The additive white gaussian noise is added after applying the channel coefficients to the signal data. We then demodulate the data packets and pass it to the ber calculator object which then computes the bit-error rate. The simulations are run for SNR values ranging from 0–20 dB and plots are generated for all three modulation schemes.

4.4 HST LTE-R in a Tunnel

Using LTE System Toolbox provided by MATLAB we generated Figure 4.4, which shows the received resource grid without equalization. The frame worth of data was modulated with QPSK, 16QAM and 64QAM for equal number of subcarriers and mapped to symbol in a subframe. We generate ten subframes individually and create one frame after merging all subframes. The frame is passed through our proposed high speed train channel model, with additive white gaussian noise added. We can see that without equalization the received resourced grid has lot of errrors and will lead to numerous retransmissions.

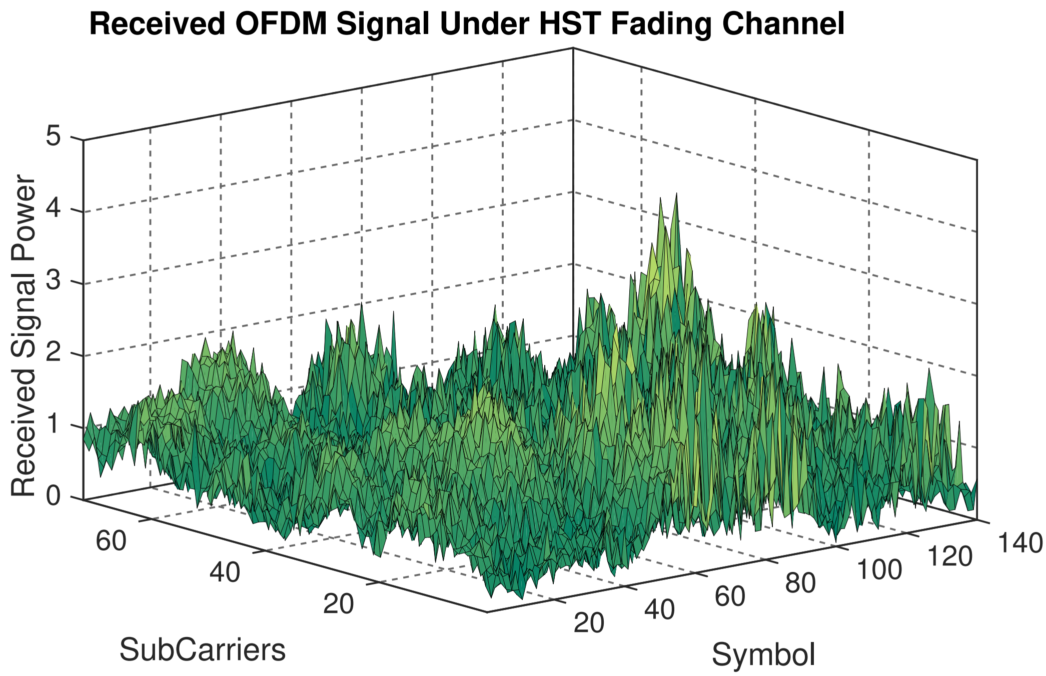

Figure 4.4: Received LTE-R OFDM signal under HST Ricean Fading Environment.

In Figure 4.5, we calculated the K-factor for the HST inside a tunnel with velocity $v =$ 500 km/h for different center frequencies. It shows the variation of the Rician K-factor with the distance between the transmitter and receiver as the train is moving along the tunnel. We computed the K-factor for a leaky cable with periodic slots separated by distance d in fixed time-steps. The plot shows that the K-factor varies significantly over a short distances. Therefore, assuming a single K-factor for the channel model is not accurate, we use time-series K-factor to do our channel modeling.

To show the impact of varying K-factor on the channel, we computed the BER curve for different modulation schemes of LTE-R with different K-factors. Figure. 4.6a shows the BER versus SNR performance for QPSK modulation for different K-factors of the tunnel channel model. The figure clearly demonstrates for higher K-factor we have a better

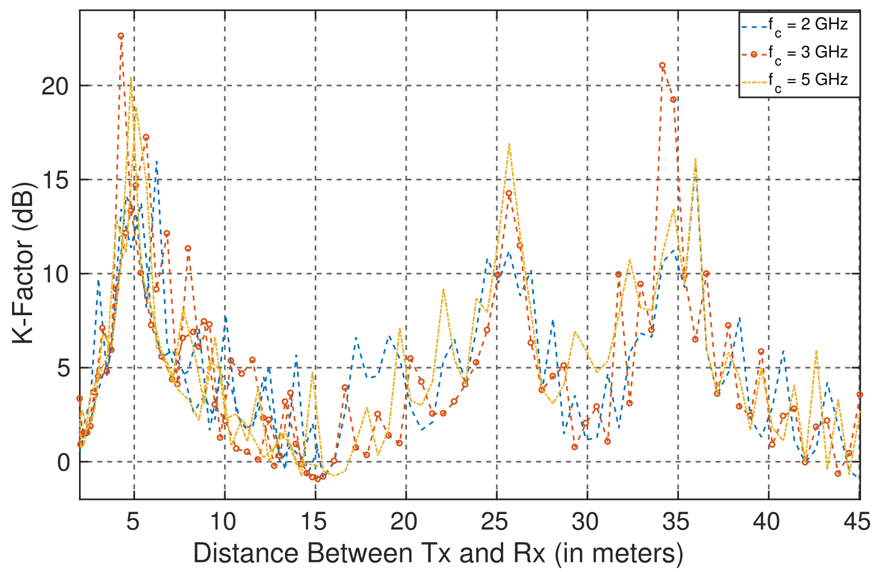

Figure 4.5: K-factor versus D_{LOS} for different center frequencies $f_c = 2$, 3 and 5 GHz.

performance while performance degrades as K-factor decreases. Figure.4.6b shows the E_b/N_0 versus BER for 16-QAM and as we can see the BER is higher compared to QPSK. Figure. 4.6c shows the E_b/N_0 versus BER for 64-QAM for different K-factors. Finally, we compare all the modulation schemes for the best and worst K-factor in Figure. 4.6d.

In Figure. 4.7 we calculate the BER performance for a high speed train in discrete time-steps. As the train moves towards the LCX slot, the SNR goes high and the SNR decreases as the train moves away. This trend can be seen in the plot, as we move towards the slot the BER curve decreases and it starts increases once we move. It is important to consider here that due to the varying nature of K-factor the BER curve also varies significantly. Hence, by considering the time-varying nature of K-factor we can have a better performance analysis.

4.5 Summary

We analyzed the BER performance of a LTE-R system for high speed trains inside tunnel environments using our proposed channel model. For the implementation of our channel, we first derived the time-series K-factor function using the classical two-ray propagation

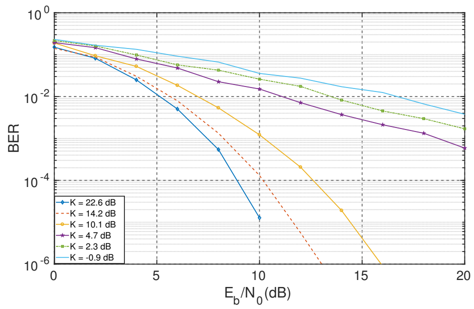

(a) OFDM-QPSK

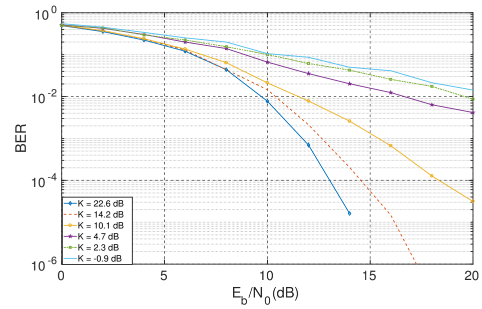

(b) OFDM-16QAM

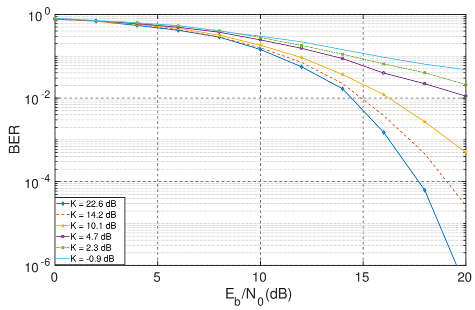

(c) OFDM-64QAM

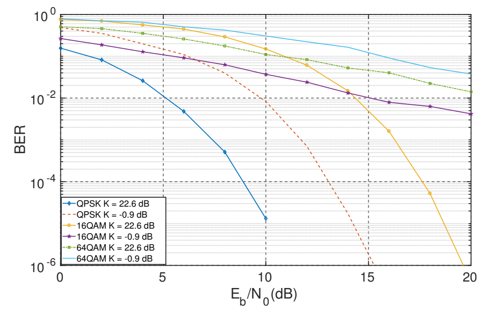

(d) OFDM-MQAM

Figure 4.6: Comparison of E_b/N_0 verus BER for LTE-R OFDM modulation with different K-factors. The first three sub-figures shows the E_b/N_0 versus BER for individual modulation schemes employed in LTE-R and in last plot we compare all the modulation schemes for different K-factors.

model. We then analyzed the LTE-R performance under our channel model for different modulation schemes for various K-factors. Finally, we compared all the modulation schemes under worst and best K-factor. The results show that for low E_b/N_0 sub-carriers must be modulated with QPSK for maintaining reliable communication link.

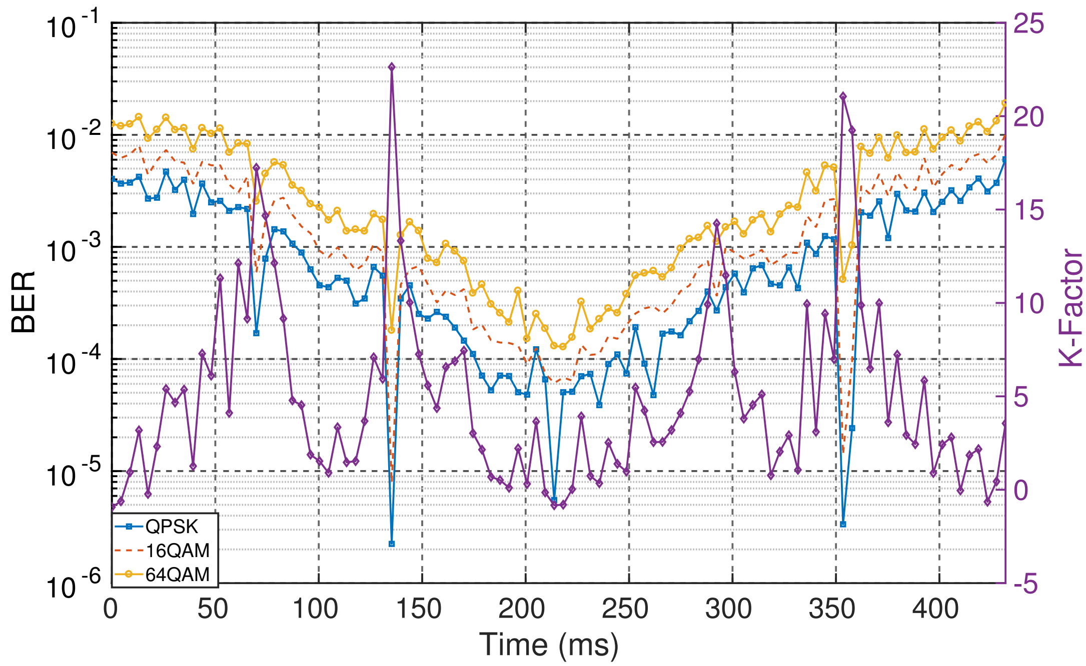

Figure 4.7: BER variation with time for HST with different modulation schemes of LTE-R. As the train moves towards the antenna the general trend of BER goes down with small-scale fluctuations due to varying K-factor.

Chapter 5

Proposed Heterogeneous CSS Prototype

5.1 Overview

This chapter outlines the implementation of heterogeneous test-bed for cooperative spectrum sensing using USRP N210 and RTL-SDR software defined radios. We start with heterogeneous cooperative spectrum sensing, where we first describe the experimental setup, which is implemented using soft and hard fusion schemes. The sensor nodes, which consists of three RTL-SDRs and one USRP N210, are placed in a controlled indoor laboratory environment approximately 8-10 meters apart. The signal source is being simulated by another USRP N210, which is transmitting a DQPSK signal at 450 MHz. The post-processing is done on a Fusion Center, which makes the decision based on global test statistic using both soft and hard decision schemes. Finally, we discuss the results where the performance of both the schemes are evaluated in a real fading scenario on a hardware test-bed.

5.2 Experimental Setup for Proposed Heterogeneous CSS Prototype

The measurements are performed using software-defined radios (SDRs) and the post-processing is conducted on desktop computers. The desktop computer consists of i7 Intel processor with eight cores and 3.41 GHz clock cycle running Ubuntu 16.04. The sensor node network is implemented using RTL-SDR dongles and Ettus Research USRP N210 on GNU Radio Software platform. The measurements are analyzed in MATLAB and measurement plots are generated. Figure 5.1 presents a photograph of the actual proposed prototype system, which consists of three RTL-SDRs and two USRP N210s. One USRP N210 (middle) acts as a primary user while the other SDRs operate as sensor nodes. All the SDRs were placed in a laboratory environment at least 5-6 meters away from the primary user.

These sensor nodes collect the spectral data, normalize it, and then transmit it to the FC for the detection. For soft data fusion, the data is quantized in the local sensor nodes before it is transmitted to FC due to the limited bandwidth of the overhead channel. The delays caused by the different sensor nodes is ignored, as it would require extra computational complexity and it is out of the scope of this thesis. The USRP N210 transmits a DQPSK modulated signal with 4 samples per symbol with the alpha factor of the root raised cosine filter set to 0.35. The transmitter gain and amplitude are varied to get different SNR values for each node. The sensor nodes collect the data for the equivalent of 300,000 energy samples, and each measurement is conducted three times to eliminate any irregularities. The noise variance σ_n^2 for each SU is estimated by running each sensor node without any transmission at 450 MHz. The flow-graph is executed multiple times to get a better estimate of noise variance. Once the data is received from all the sensor nodes, the Probability of Detection (P_d) is calculated for different received SNR values for all the sensor nodes. To properly evaluate the performance of each of the cooperative spectrum sensing techniques, the average P_d is calculated for each scheme.

All four sensor nodes have different sampling rates to model potential differences existing within a heterogeneous environment. The USRP N210, which is also used as a 4^{th} sensor node, has a very low noise floor compared to the three other radios and hence can detect a

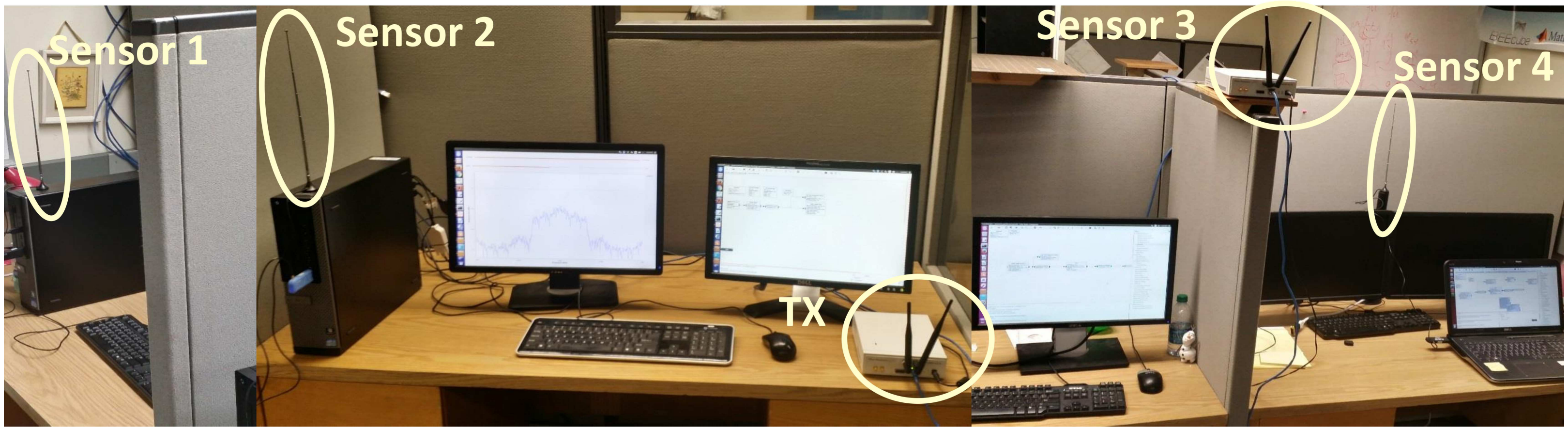

Figure 5.1: Experimental Test-Bed For Cooperative Sensing in Heterogeneous Network. Sensors 1, 2 and 4 are RTL-SDR units, sensor 3 is USRP N210 and TX is another USRP N210 unit which is used as a signal source for this work.

signal with very low SNR. This is a challenging factor for data fusion when the nodes have different operating parameters and the FC has to make optimal decisions by combining this varying data. Due to their spatial diversity, the node closest to the transmitter will have different SNR compared to the other nodes. All these factors impact the data combining at FC. The GNU Radio flow-graph for the sensor nodes is shown in the Figure 5.3. The same flow-graph is used for all sensor nodes with different operating parameters. For the USRP N210 node, we replaced the RTL-SDR source with UHD:USRP Source gnuradio block. The central frequency is kept at 450 MHz and the operating parameters of each sensor node is provided in Table 5.1. The values of the transmitter amplitude and gain are varied to get the different sets of SNR values which are used for computing P_d values for each node. The plots are generated in MATLAB by using the data files from the GNU Radio platform.

To evaluate the performance of the cooperative spectrum sensing, the USRP N210 is used as a transmitter, where its gain and amplitude are varied. Figure 5.2 shows the flow-graph used for the transmitter. The flow-graph starts with the random source block, which generates the random data between zero and three, and passes it to the differential phase shift keying (DPSK) modulator block. The DPSK block modulates the signal with differential quadrature phase shift keying (DQPSK) scheme, applies root raise cosine filter with excess bandwidth value of 0.35, and passes it to a multiply const block. It is used to control the SNR value and finally the data is dumped into the USRP N210 sink, which transmits the data over the air where other sensor nodes can estimate the signal presence using soft and hard decision schemes.

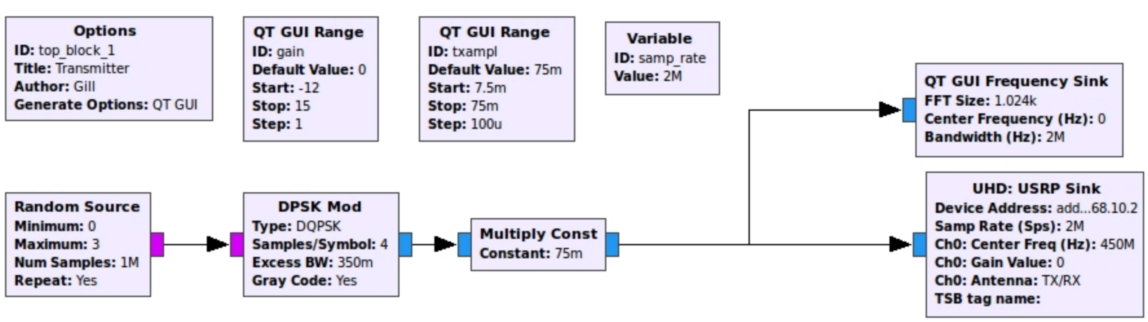

Figure 5.2: GNU Radio Flowgraph For Transmitter Running on USRP N210.

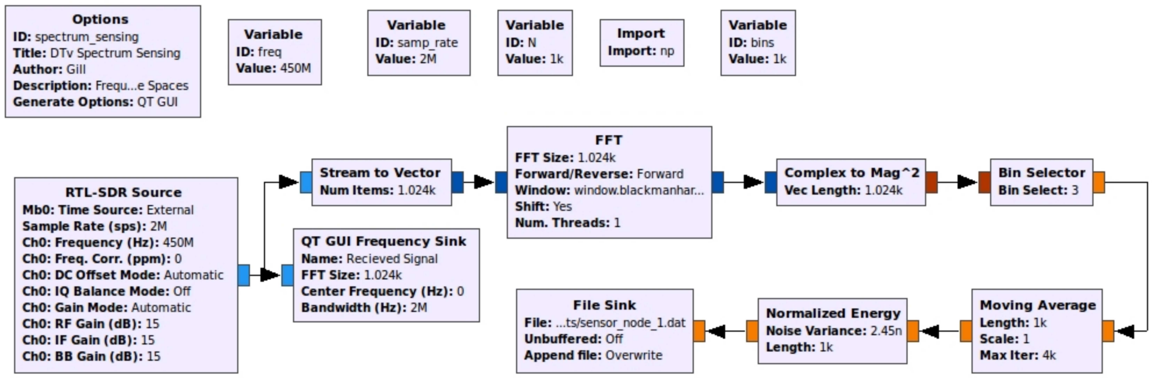

Figure 5.3: GNURadio Flowgraph For USRP and RTL-SDR sensor nodes.

Table 5.1: Operating Characteristics of Sensor Nodes

Nodes	F_s	Gain	FFT Size	Bin Size
RTL-SDR-1	1.1 Msps	10 dB	512	2.148 KHz
RTL-SDR-2	1.8 Msps	10 dB	512	3.515 KHz
RTL-SDR-3	2.4 Msps	10 dB	512	4.687 KHz
USRP N210	7.2 Msps	10 dB	512	14.062 KHz

The sensor nodes are placed inside the laboratory and are connected to distributed system. Figure 5.3 shows the flowgraph running on the receiver, for flow-graph running on USRP we use UHD:USRP source instead of RTL-SDR source. The frequency around 450 MHz is sweeped in regular intervals and the continuous data stream is passed to FFT block, which does the forward FFT operation with Blackmann Harris window. The data is first converted into parallel stream of the FFT size using stream to vector GNU Radio block. We complex to magnitude block converts the complex values into float and take their magnitude. The bin selector block is used to select the bin where the narrowband signal is being transmitted by the transmitter. We then take the moving average of the values, normalize them and then store it to the file sink. The normalized energy values are collected for each sensor at different SNR values and then post processing is performed in MATLAB. The operating parameters of each sensor node is provided in the Table **??**.

5.3 Hard-Data Fusion Scheme

Cooperative spectrum sensing using hard-data fusion is a proven method for improving the detection performance. In this scheme, all sensor nodes sense the signal source individually and send their sensing decision in the form of 1-bit binary data. For hard data fusion, the noise w_q can be neglected since the sensor nodes can just transmit their decision statistic in an efficient way, where the floating values are not required. For example, the SUs can just transmit "1" and "0" depending on whether the primary user is present or absent. Furthermore, in the Fusion Center the decision can be made by using the OR, AND, or majority rule algorithms. For the AND decision rule, the FC performs the logical AND operation for all the local decisions and conducts the detection. Similarly, for the OR rule, the logical OR operation is used to decide whether the signal is present or not. Finally, the majority rule conducts majority vote and decides based on it [72,73]. The P_d for AND, OR and Majority Rule for $R = 4$ sensor nodes is given by [74]:

$$\begin{gathered} P_{d,AND} = (P_d)^4 \\ P_{d,OR} = 1 - (1 - P_d)^4 \\ P_{d,MJR} = 6P_{davg}^2(1 - P_{davg})^2 + 4P_{davg}^3(1 - P_{davg}) + P_{davg}^4 \end{gathered} \tag{5.1}$$

where P_{davg} is the average probability of detection of the sensor units. Similarly, we can calculate the P_{fa} for all three schemes by replacing P_{davg} by P_{faavg} in Eq (5.4).

5.4 Soft-Data Fusion Scheme

In soft-data fusion based cooperative spectrum sensing, information from different CR users is combined to make a decision on the presence or absence of the primary user. In Section 5.3, we discussed the conventional hard combination, where each CR user feedbacks one-bit message regarding whether observed energy is above a certain threshold. In this section, we discuss soft combination of the local test statistic of each sensor nodes and how it is combined to make the decision in the FC. Since in the soft combination accurate energy values from different CR users are utilized to make a decision, this scheme is more accurate and complex to implement. In this thesis, we discuss two popular soft decision

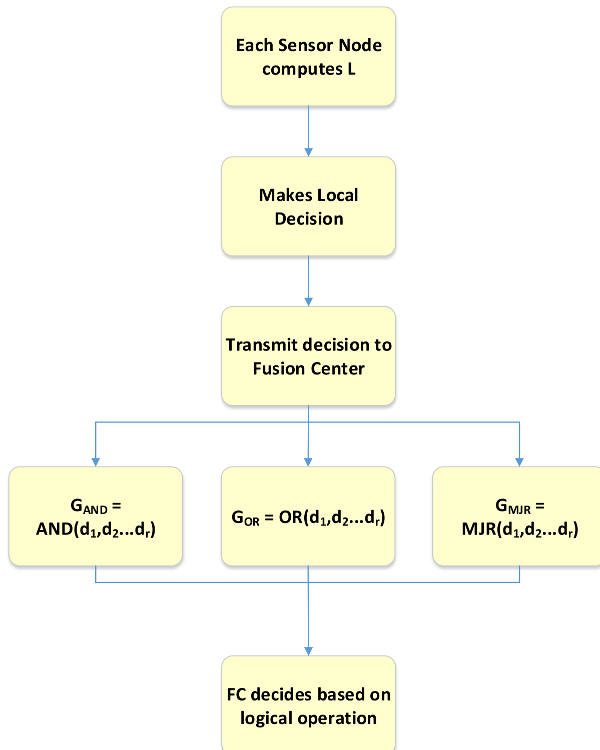

Figure 5.4: Flowchart showing AND, OR and Majority Rule Fusion schemes.

fusion schemes: *Maximum Normalized Energy* (MNE) scheme and *Equal Gain Combining* (EGC) scheme.

For MNE, the local test statistic in each sensor node is computed and then transmitted to FC after quantization. In this thesis, we are using four sensor nodes equipped with different sensing abilities such as the sampling rates and noise floor. Therefore, the global test statistic G can be modeled by:

$$G_{MNE} = \max\{\beta_r\}. \tag{5.2}$$

The P_{fa} and P_d values for the MNE-CS is given by [25]:

$$P_{fa} = 1 - \prod_{r=1}^{R}\left(1 - Q\left(\frac{\tau - 1}{\sqrt{\frac{1}{M_r} + \sigma_{q,r}}}\right)\right), \tag{5.3}$$

$$P_d = 1 - \prod_{r=1}^{R}\left(1 - Q\left(\frac{\tau - 1 - \gamma_r}{\sqrt{\frac{1 + 2\gamma_r}{M_r} + \sigma_{q,r}}}\right)\right), \tag{5.4}$$

where τ is the global threshold for MNE, M_r is the number of samples for r^{th} sensor node, and $\sigma_{q,r}$ is the noise variance for the received local test statistic. The algorithm for MNE-CS is illustrated by the flowchart in Figure 5.5.

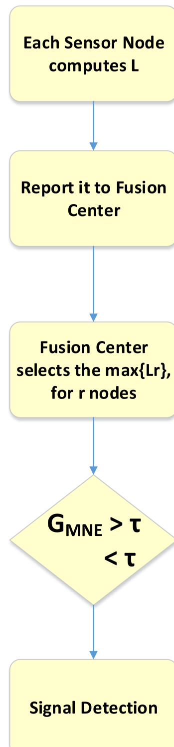

Figure 5.5: Flowchart describing Maximum Normalized Energy Scheme.

For EGC, the global decision statistic is the mean of the β values for all the sensor nodes. It has been shown in [25] that the EGC scheme performs better than the MNE scheme in a noisy channel. The EGC scheme can be modeled by:

$$G_{EGC} = \frac{1}{M} \sum_{r=1}^{M} \beta_r, \tag{5.5}$$

where G_{EGC} is global test statistic of EGC scheme. The P_{fa} and P_d values for the EGC-CS scheme are given by:

$$P_{fa} = Q\left(\frac{\tau - 1}{\sqrt{\frac{1}{R^2} \sum_{r=1}^{R} \left(\frac{1}{M_r} + \sigma_{q,r}^2 \right)}} \right), \tag{5.6}$$

$$P_d = Q\left(\frac{\tau - \frac{1}{R}\sum_{r=1}^{R}(1+\gamma_r)}{\sqrt{\frac{1}{R^2}\sum_{r=1}^{R}\left(\frac{1+2\gamma_r}{M_r}+\sigma_{q,r}^2\right)}}\right). \tag{5.7}$$

The algorithm for EGC-CS is also illustrated by the flowchart in Figure 5.6.

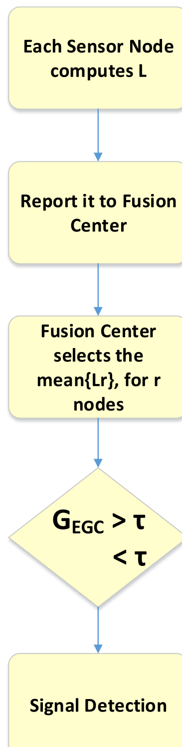

Figure 5.6: Flowchart describing Equal Gain Combining Scheme.

5.5 Heterogeneous CSS Experimental Results

In this thesis, we implemented the heterogeneous cooperative spectrum sensing (CSS) using both hard and soft data fusion schemes. We start by collecting the data across 450 MHz band for all sensor nodes in a distributed manner. The spectrum sensing data is normalized for both soft and hard data fusion schemes using the same operational parameters to compare their performance accurately. The measurements are performed using software-defined radios (SDRs) and the post processing is conducted on desktop computers. The desktop computer consists of an i7 Intel processor with eight cores and 3.41 GHz clock cycle running Ubuntu 16.04. The sensor node network is implemented using RTL-SDR dongles and Ettus Research USRP N210 on GNU Radio Software platform. These sensor nodes collect the spectral data, normalize it and then transmit it to the FC for the detection. For soft data fusion, the data is quantized in the local sensor nodes before it is transmitted to FC due to the limited bandwidth of the overhead channel.

Figure 5.7 shows the P_{davg} versus SNR_{avg} for all four sensor nodes when hard decision combining is performed. It can be seen that OR performs the best, while AND performs the worst in a fading channel. The SNR average was computed by taking the mean of all the SNRs for the sensor nodes. The SNR was varied for each sensor node by varying the transmitter amplitude and gain in the GNU Radio flow-graph.

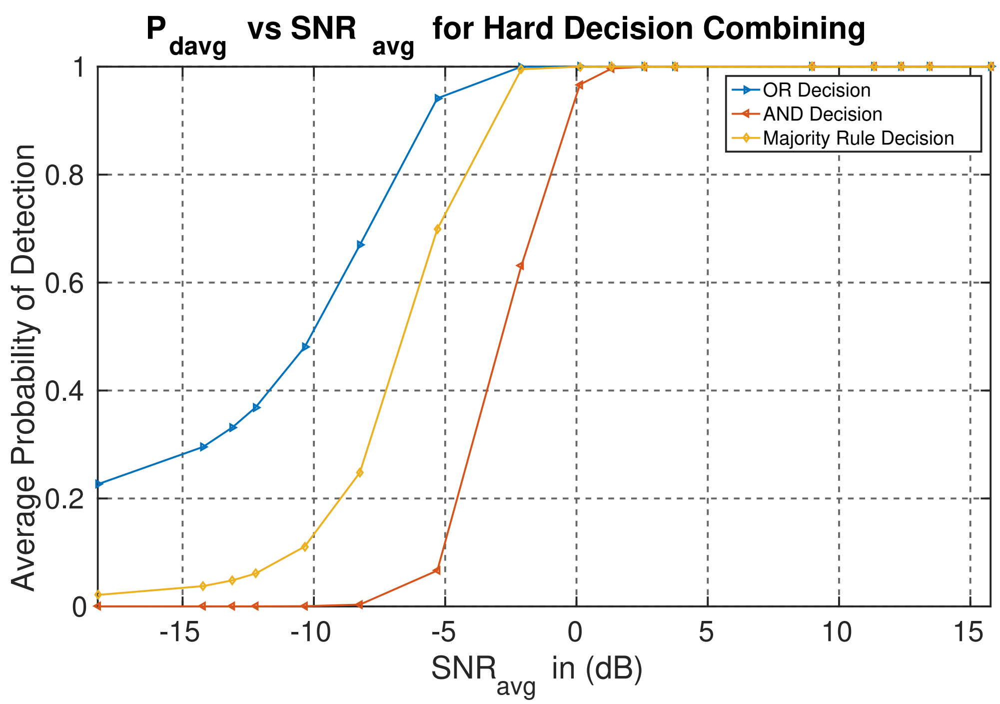

Figure 5.7: Probability of Detection versus SNR_avg For Hard Decision Combining.

In Figure 5.8, the ROC characteristics for the hard decision combining at two different SNR_{avg} for all three hard data fusion schemes are provided. It is pretty evident from the plot that the OR scheme performs better than both the AND and majority rule schemes.

The AND scheme performs the worst because it depends on all sensor nodes to have same decision, which is very difficult in a real fading environment. For lower SNR values, OR outperform the majority rule by a large margin but as we go to higher SNR values their performance converges.

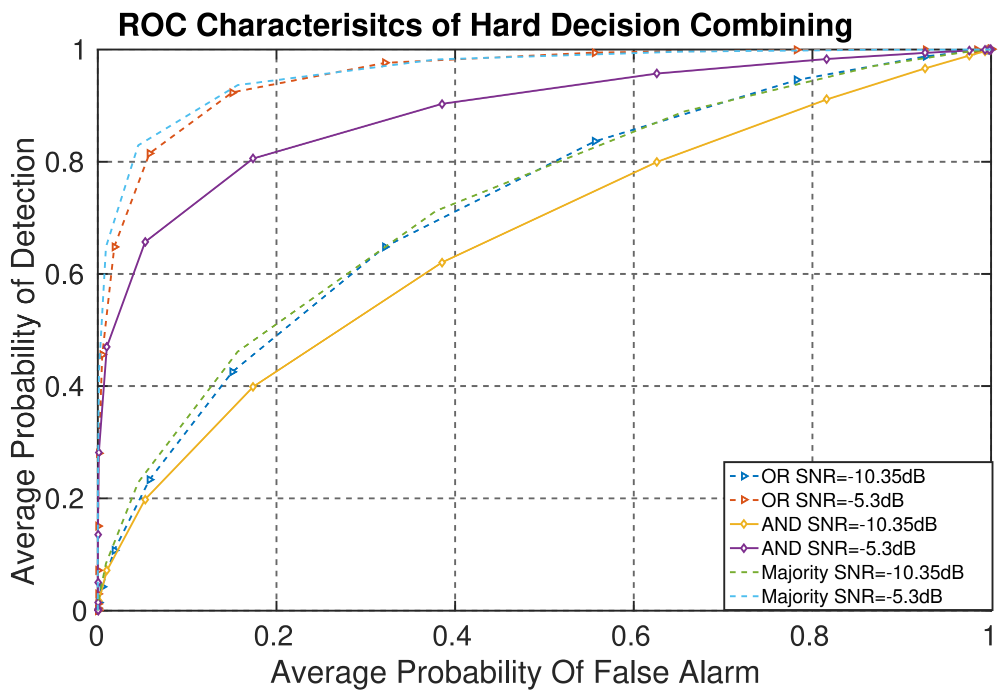

Figure 5.8: ROC Characteristics for Hard Decision Combining with Different SNRs.

The Figure 5.9 shows the P_{davg} versus SNR_{avg} for both soft and hard data fusion schemes. MNE and OR schemes overlap on the plot because in MNE scheme we take the maximum normalized energy and compare it the global test statistic, whereas for the OR scheme we estimate the signal source by either of sensor node decision. This makes both the scheme almost same and this is visible in the results. The EGC scheme performs the best because it takes into consideration all the sensor nodes and its global test statistic gives equal weight to all sensor nodes. The AND scheme performs the worst as expected. It is very important to understand that at higher SNR values, $SNR_{avg} > 2$ dB, we see all schemes converging to the same decisions. This tells us that in noiseless environment, we can choose hard fusion schemes because of their implementation complexity and we can select soft fusion in severe fading environment as they tend to be more accurate in these scenarios.

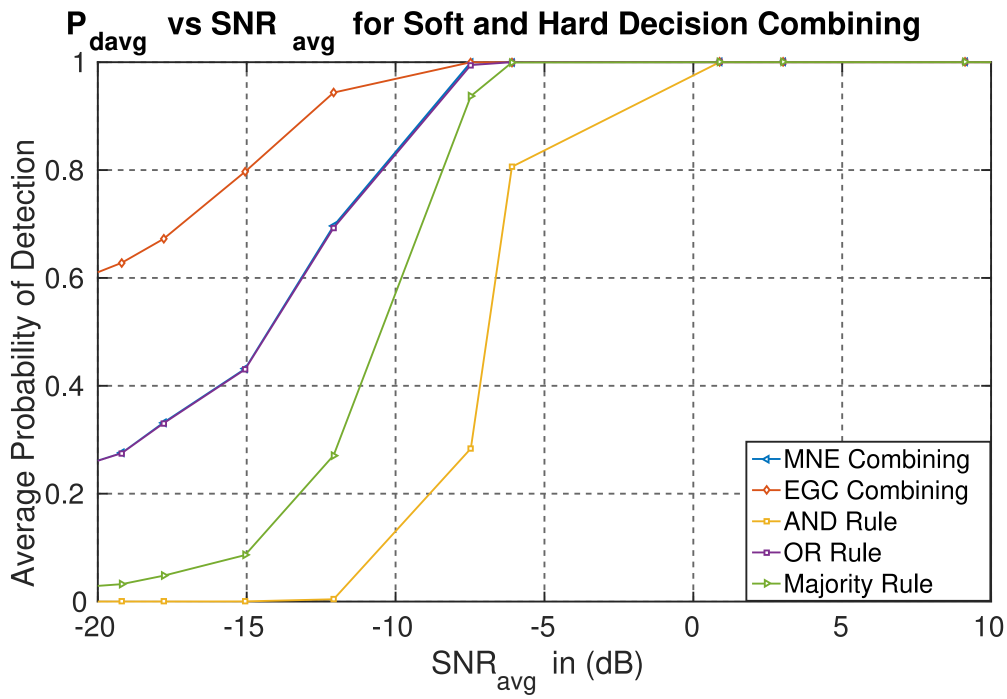

Figure 5.9: Probability of Detection versus SNR_avg For Soft and Hard Decision Combining.

5.6 Summary

In this chapter, we described the test-bed setup using USRP N210 and RTL-SDR with different operating characteristics. The proposed heterogeneous CSS performance for both soft and hard data fusion approaches was derived at different SNR values. For soft-data fusion, scheme we use maximum normalized energy (MNE) and equal gain combining (EGC) scheme, and for hard data fusion scheme we used AND, OR and Majority Rule approaches. The results show that soft-data fusion scheme performs better than hard data fusion schemes for low SNR values, but as we increase SNR both schemes converges to same values. We learned that for severe environment, we can use soft-fusion and for noise-free environment hard decision schemes can be used due to their low implementation complexity.

Chapter 6

Conclusions

The research achievements of this thesis includes a simulation test-bed that is implemented in MATLAB in order to test the performance of LTE-R in our proposed channel. The proposed channel is built on two-ray propagation model with time-series K-factor, which we have derived mathematically and also uses Doppler shift profile for high speed trains. We also discussed the implementation of a test-bed for cooperative spectrum sensing in heterogeneous networks, the performance measure of both soft and hard data fusion schemes in a real fading scenario.

6.1 Research Outcomes

- We analyzed the BER performance of a LTE-R system for high speed trains inside tunnel environments using our proposed channel model. For the implementation of our channel, we first derived the time-series K-factor function using the classical two-ray propagation model.

- We analyzed the LTE-R performance under our channel model for different modulation schemes for various K-factors. We also compared all the modulation schemes under worst and best K-factor, and we observed that for low E_b/N_0 sub-carriers must be modulated with QPSK for maintaining reliable communication link.

- We obtained the BER curve for discrete time-step when the train is moving with a velocity of 500 Km/h and carrier frequency for all modulation scheme is set to 3 GHz. The plot is also overlayed with continuous K-factor variation with the propagation of the train. It can be observed from the plot that as the K-factor goes high the BER drops, which represents the train moving towards the LCX slot. As the train move away from the slot the BER starts increasing. For reliable and efficient communication links the sub-carriers have to be modulated with QPSK for low K-factor values, or more LTE repeaters are required inside the tunnel to get good connectivity. However, the most important factor that has to be taken into consideration is the real-time channel equalization to reduce the BER rate.

- We also conducted an experimental study for cooperative spectrum sensing using normalized energy detection for both soft and hard decision combining techniques. It was found that the soft fusion schemes works better than hard decision for real fading environment with low SNR values. For higher values, all schemes converged to the same decision which led us to conclude that hard fusion schemes pays better when the environment is less noisy due to their low complexity as compared to soft fusion.

6.2 Future Work

For future work we will use LTE toolbox in MATLAB which gives more realistic picture of the simulation environment and we will expand the channel model to cover more scenarios for high speed railway. In heterogeneous cooperative spectrum sensing it is worth exploring an increase in the number of nodes and adding mobility for the testing the performance of heterogeneous networks in a time-variant channel.

Bibliography

[1] FCC Frequency Allocation Chart. [Online]. Available: https://www.ntia.doc.gov/page/2011/united-states-frequency-allocation-chart

[2] H. Wang, F. R. Yu, and H. Jiang, "Modeling of radio channels with leaky coaxial cable for lte-m based cbtc systems," *IEEE Communications Letters*, vol. 20, no. 5, pp. 1038–1041, 2016.

[3] A. M. Wyglinski and D. Pu, *Digital communication systems engineering with software-defined radio*. Artech House, 2013.

[4] "Corridor: Cognitive radio for railway through dynamic and opportunistic spectrum reuse." March 2014. [Online]. Available: http://corridor.ifsttar.fr

[5] A. Amanna, M. Gadnhiok, M. J. Price, J. H. Reed, W. P. Siriwongpairat, and T. K. Himsoon, "Railway cognitive radio," *IEEE Vehicular Technology Magazine*, vol. 5, no. 3, pp. 82–89, Sept 2010.

[6] U. G. Functional Group, "GSM-R functional requirement specification (FRS)," UIC, Paris, France UIC EIRENE Technology Report, Tech. Rep. UIC Code 950, Version 7.3.0, 2012.

[7] G. T. 36.201, "Evolved universal terrestrial radio access (E-UTRA); LTE physical layer; general description," 3GPP, Sophia Antipolis, France, Tech. Rep. version 12.2.0, Release 12, 2015.

[8] K. Masur and D. Mandoc, "LTE/SAE the future railway mobile radio system? long

term visions on railway mobile radio technologies," *International Union of Railways (UIC), Technical Report*, vol. 1, 2009.

[9] G. Tingting and S. Bin, "A high-speed railway mobile communication system based on lte," in *Electronics and Information Engineering (ICEIE), 2010 International Conference On*, vol. 1. IEEE, 2010, pp. V1–414.

[10] K. Guan, Z. Zhong, and B. Ai, "Assessment of lte-r using high speed railway channel model," in *Communications and Mobile Computing (CMC), 2011 Third International Conference on*. IEEE, 2011, pp. 461–464.

[11] H. Wei, Z. Zhong, K. Guan, and B. Ai, "Path loss models in viaduct and plain scenarios of the high-speed railway," in *Communications and Networking in China (CHINACOM), 2010 5th International ICST Conference on*. IEEE, 2010, pp. 1–5.

[12] D. G. Dudley, M. Lienard, S. F. Mahmoud, and P. Degauque, "Wireless propagation in tunnels," *IEEE Antennas and Propagation Magazine*, vol. 49, no. 2, pp. 11–26, 2007.

[13] I. F. Akyildiz, W.-Y. Lee, M. C. Vuran, and S. Mohanty, "Next generation/dynamic spectrum access/cognitive radio wireless networks: A survey," *Computer networks*, vol. 50, no. 13, pp. 2127–2159, 2006.

[14] Q. Zhao and B. M. Sadler, "A survey of dynamic spectrum access," *IEEE signal processing magazine*, vol. 24, no. 3, pp. 79–89, 2007.

[15] H. Urkowitz, "Energy detection of unknown deterministic signals," *Proceedings of the IEEE*, vol. 55, no. 4, pp. 523–531, 1967.

[16] D. Cabric, S. M. Mishra, and R. W. Brodersen, "Implementation issues in spectrum sensing for cognitive radios," in *Signals, systems and computers, 2004. Conference record of the thirty-eighth Asilomar conference on*, vol. 1. Ieee, 2004, pp. 772–776.

[17] R. Tandra and A. Sahai, "Fundamental limits on detection in low snr under noise uncertainty," in *Wireless Networks, Communications and Mobile Computing, 2005 International Conference on*, vol. 1. IEEE, 2005, pp. 464–469.

[18] S. M. Mishra, A. Sahai, and R. W. Brodersen, "Cooperative sensing among cognitive radios," in *Communications, 2006. ICC'06. IEEE International conference on*, vol. 4. IEEE, 2006, pp. 1658–1663.

[19] A. Ghasemi and E. S. Sousa, "Impact of user collaboration on the performance of sensing-based opportunistic spectrum access," in *Vehicular Technology Conference, 2006. VTC-2006 Fall. 2006 IEEE 64th*. IEEE, 2006, pp. 1–6.

[20] J.-M. Molina-Garcia-Pardo, M. Lienard, A. Nasr, and P. Degauque, "Wideband analysis of large scale and small scale fading in tunnels," in *ITS Telecommunications, 2008. ITST 2008. 8th International Conference on*. IEEE, 2008, pp. 270–273.

[21] T. Liu, X. Ma, R. Zhao, H. Dong, and L. Jia, "Doppler shift estimation for high-speed railway scenario," in *2016 IEEE 83rd Vehicular Technology Conference (VTC Spring)*, May 2016, pp. 1–5.

[22] J. Ma, G. Zhao, and Y. Li, "Soft combination and detection for cooperative spectrum sensing in cognitive radio networks," *IEEE Transactions on Wireless Communications*, vol. 7, no. 11, pp. 4502–4507, 2008.

[23] B. Shen, T. Cui, K. Kwak, C. Zhao, and Z. Zhou, "An optimal soft fusion scheme for cooperative spectrum sensing in cognitive radio network," in *Wireless Communications and Networking Conference, 2009. WCNC 2009. IEEE*. IEEE, 2009, pp. 1–5.

[24] H. Rifà-Pous, M. J. Blasco, and C. Garrigues, "Review of robust cooperative spectrum sensing techniques for cognitive radio networks," *Wireless Personal Communications*, vol. 67, no. 2, pp. 175–198, 2012.

[25] Y. Zeng, Y.-C. Liang, S. Zheng, and E. C. Peh, "Optimal cooperative sensing and its robustness to decoding errors," in *Communications (ICC), 2011 IEEE International Conference on*. IEEE, 2011, pp. 1–5.

[26] T. S. Rappaport *et al.*, *Wireless communications: principles and practice*. prentice hall PTR New Jersey, 1996, vol. 2.

[27] USRP. [Online]. Available: https://www.ettus.com/product/category/USRP-Embedded-Series/

[28] RTL-SDR. [Online]. Available: http://www.rtl-sdr.com/

[29] R. Lindsey, "Positive train control in north america," *IEEE Vehicular Technology Magazine*, vol. 4, no. 4, pp. 22–26, December 2009.

[30] "WiBro standard PhaseI," December 2004, tTAS.KO-06.0065R1. [Online]. Available: http://corridor.ifsttar.fr

[31] G. Tingting and S. Bin, "A high-speed railway mobile communication system based on LTE," in *Electronics and Information Engineering (ICEIE), 2010 International Conference On*, vol. 1. IEEE, 2010, pp. V1–414.

[32] F. Rusek, D. Persson, B. K. Lau, E. G. Larsson, T. L. Marzetta, O. Edfors, and F. Tufvesson, "Scaling up MIMO: Opportunities and challenges with very large arrays," *IEEE Signal Processing Magazine*, vol. 30, no. 1, pp. 40–60, 2013.

[33] R. He, B. Ai, G. Wang, K. Guan, Z. Zhong, A. F. Molisch, C. Briso-Rodriguez, and C. P. Oestges, "High-speed railway communications: From GSM-R to LTE-R," *IEEE Vehicular Technology Magazine*, vol. 11, no. 3, pp. 49–58, Sept 2016.

[34] A. M. Wyglinski, M. Nekovee, and T. Hou, *Cognitive radio communications and networks: principles and practice*. Academic Press, 2009.

[35] S. Haykin, "Cognitive radio: brain-empowered wireless communications," *IEEE journal on selected areas in communications*, vol. 23, no. 2, 2005.

[36] X. Hong, C.-X. Wang, M. Uysal, X. Ge, and S. Ouyang, "Capacity of hybrid cognitive radio networks with distributed VAAs," *IEEE Transactions on Vehicular Technology*, vol. 59, no. 7, pp. 3510–3523, 2010.

[37] X. Ge, H. Cheng, G. Mao, Y. Yang, and S. Tu, "Vehicular communications for 5G cooperative small-cell networks," *IEEE Transactions on Vehicular Technology*, vol. 65, no. 10, pp. 7882–7894, 2016.

[38] P. Unterhuber, S. Sand, M. Soliman, B. Siebler, A. Lehner, T. Strang, M. d'Atri, F. Tavano, and D. Gera, "Wide band propagation in train-to-train scenarios-Measurement campaign and first results," in *Antennas and Propagation (EUCAP), 2017 11th European Conference on*. IEEE, 2017, pp. 3356–3360.

[39] P. Unterhuber, S. Pfletschinger, S. Sand, M. Soliman, T. Jost, A. Arriola, I. Val, C. Cruces, J. Moreno, J. P. García-Nieto *et al.*, "A survey of channel measurements and models for current and future railway communication systems," *Mobile Information Systems*, vol. 2016, 2016.

[40] S. Mumtaz, K. M. S. Huq, and J. Rodriguez, "Direct mobile-to-mobile communication: Paradigm for 5G," *IEEE Wireless Communications*, vol. 21, no. 5, pp. 14–23, 2014.

[41] K. Noritaka, N. Takena, and N. Tsunw, "Leaky coaxial cable," May 7 1974, US Patent 3,810,186. [Online]. Available: https://www.google.com/patents/US3810186

[42] A. Motley and D. Palmer, "Directed radio coverage within buildings," in *Proc. IEE Conf. Radio spectrum conversion techniques*, 1983.

[43] A. A. Saleh, A. Rustako, and R. Roman, "Distributed antennas for indoor radio communications," *IEEE Transactions on Communications*, vol. 35, no. 12, pp. 1245–1251, 1987.

[44] H. Cao and Y. Zhang, "Radio propagation along a radiated mode leaky coaxial cable in tunnels," in *Microwave Conference, 1999 Asia Pacific*, vol. 2. IEEE, 1999, pp. 270–272.

[45] T. Takatsu, "The history and future of high-speed railways in japan," *Japan Railway & Transport Review*, vol. 48, pp. 6–21, 2007.

[46] K. Hassan, I. Dayoub, W. Hamouda, C. N. Nzeza, and M. Berbineau, "Blind digital modulation identification for spatially-correlated MIMO systems," *IEEE Transactions on Wireless Communications*, vol. 11, no. 2, pp. 683–693, 2012.

[47] S. Kharbech, I. Dayoub, E. Simon, and M. Zwingelstein-Colin, "Blind digital modulation detector for MIMO systems over high-speed railway channels," in *International Workshop on Communication Technologies for Vehicles*. Springer, 2013, pp. 232–241.

[48] K. Hassan, I. Dayoub, W. Hamouda, and M. Berbineau, "Automatic modulation recognition using wavelet transform and neural network," in *Intelligent Transport Systems Telecommunications,(ITST), 2009 9th International Conference on*. IEEE, 2009, pp. 234–238.

[49] E. P. Simon and M. A. Khalighi, "Iterative soft-kalman channel estimation for fast time-varying MIMO-OFDM channels," *IEEE Wireless Communications Letters*, vol. 2, no. 6, pp. 599–602, 2013.

[50] K. Gill and A. Wyglinski, "Heterogeneous cooperative spectrum sensing test-bed using software-defined radios," in *2017 IEEE 86th Vehicular Technology Conference (VTC-Fall)*. IEEE, 2017.

[51] F. Weidling, D. Datla, V. Petty, P. Krishnan, and G. Minden, "A framework for RF spectrum measurements and analysis," in *New Frontiers in Dynamic Spectrum Access Networks, 2005. DySPAN 2005. 2005 First IEEE International Symposium on*. IEEE, 2005, pp. 573–576.

[52] J. Mitola and G. Q. Maguire, "Cognitive radio: making software radios more personal," *IEEE Personal Communications*, vol. 6, no. 4, pp. 13–18, Aug 1999.

[53] B. Barker, A. Agah, and A. M. Wyglinski, "Mission-oriented communications properties for software-defined radio configuration," *Cognitive Radio Networks*, p. 435, 2008.

[54] T. R. Newman, B. A. Barker, A. M. Wyglinski, A. Agah, J. B. Evans, and G. J. Minden, "Cognitive engine implementation for wireless multicarrier transceivers," *Wireless communications and mobile computing*, vol. 7, no. 9, pp. 1129–1142, 2007.

[55] T. R. Newman, R. Rajbanshi, A. M. Wyglinski, J. B. Evans, and G. J. Minden, "Population adaptation for genetic algorithm-based cognitive radios," *Mobile networks and applications*, vol. 13, no. 5, pp. 442–451, 2008.

[56] G. Yang, J. Wang, J. Luo, O. Y. Wen, H. Li, Q. Li, and S. Li, "Cooperative spectrum sensing in heterogeneous cognitive radio networks based on normalized energy detection," *IEEE Transactions on vehicular technology*, vol. 65, no. 3, pp. 1452–1463, 2016.

[57] Y. Zeng and Y.-C. Liang, "Eigenvalue-based spectrum sensing algorithms for cognitive radio," *IEEE transactions on communications*, vol. 57, no. 6, 2009.

[58] J. Mitola, "Software radios-survey, critical evaluation and future directions," in *[Proceedings] NTC-92: National Telesystems Conference*, May 1992, pp. 13/15–13/23.

[59] R. I. Lackey and D. W. Upmal, "Speakeasy: the military software radio," *IEEE Communications Magazine*, vol. 33, no. 5, pp. 56–61, May 1995.

[60] Xilinx-Spartan-3A. [Online]. Available: https://www.xilinx.com/products/silicon-devices/fpga/xa-spa

[61] GNU Radio. [Online]. Available: http://gnuradio.org/

[62] MATLAB2017a. [Online]. Available: https://www.mathworks.com/products/matlab.html

[63] D. L. Tennenhouse and V. G. Bose, "Spectrumware: A software-oriented approach to wireless signal processing," in *Proceedings of the 1st Annual International Conference on Mobile Computing and Networking*, ser. MobiCom '95. New York, NY, USA: ACM, 1995, pp. 37–47. [Online]. Available: http://doi.acm.org/10.1145/215530.215551

[64] V. Bose, M. Ismert, M. Welborn, and J. Guttag, "Virtual radios," *IEEE Journal on selected areas in communications*, vol. 17, no. 4, pp. 591–602, 1999.

[65] T. F. Collins, "Implementation and analysis of spectral subtraction and signal separation in deterministic wide-band anti-jamming scenarios," Ph.D. dissertation, Worcester Polytechnic Institute, 2013.

[66] M. Pätzold, *Mobile radio channels.* John Wiley & Sons, 2011.

[67] F. F. Digham, M.-S. Alouini, and M. K. Simon, "On the energy detection of unknown signals over fading channels," in *Communications, 2003. ICC'03. IEEE International Conference on*, vol. 5. Ieee, 2003, pp. 3575–3579.

[68] 3rd Generation Partnership Project, "Technical specification group radio access network; Spatial channel model for MIMO simulations," 3GPP, Sophia Antipolis, France, Tech. Rep. TR 25.996 V6.1.0, 2003.

[69] P. V. R. Ferreira and A. M. Wyglinski, "Performance analysis of UHF mobile satellite communication system experiencing ionospheric scintillation and terrestrial multipath fading," in *Vehicular Technology Conference (VTC Fall), 2015 IEEE 82nd*. IEEE, 2015, pp. 1–5.

[70] D. Jordane *et al.*, *Electromagnetic waves and radiating systems.* Prentice-Hall Of Lndia Private Limited; New Delhi, 1967.

[71] K. Arshad, F. Katsriku, A. Lasebae *et al.*, "Effects of different parameters on attenuation rates in circular and arch tunnels," *PIERS Online*, vol. 3, no. 5, pp. 607–611, 2007.

[72] A. Ghasemi and E. S. Sousa, "Collaborative spectrum sensing for opportunistic access in fading environments," in *New Frontiers in Dynamic Spectrum Access Networks, 2005. DySPAN 2005. 2005 First IEEE International Symposium on.* IEEE, 2005, pp. 131–136.

[73] J. Duan and Y. Li, "Performance analysis of cooperative spectrum sensing in different fading channels," in *Computer Engineering and Technology (ICCET), 2010 2nd International Conference on*, vol. 3. IEEE, 2010, pp. V3–64.

[74] S. Nallagonda, S. D. Roy, A. Chandra, and S. Kundu, "Performance of cooperative spectrum sensing in hoyt fading channel under hard decision fusion rules," in *Computers and Devices for Communication (CODEC), 2012 5th International Conference on.* IEEE, 2012, pp. 1–4.

Appendix A

Heterogeneous Cooperative Spectrum Sensing Code

A.1 harddecisionpdroc.m

```
% Hard-Decision Combining Results For Sensor Nodes
clc;
close all;
clear all;
%% Parameter Initialization
N = 32;
k=4;%sensor nodes..
variance = 24.32e-9;
pfa = 0.05;
threshold = (qfuncinv(pfa)+sqrt(N)).*sqrt(N)*2*variance;
snrthreotical = -18:0.5:20;
snrlinear = 10.^(snrthreotical/10);
%% SNR values from USRP and RTL-SDR
snrpracticalavg = [-18.23,-14.22,-13.1,-12.22,-10.35,-8.25,-5.3,-2.1,0.13,...
    1.34,2.58,3.76,8.98,11.33,12.35,13.45,15.77];
snrlinearprac = 10.^(snrpracticalavg/10);
%% Computing Detection Probability and ROC Characteristics
```

```
pdprac = qfunc((threshold-2*N*variance.*(1+snrlinearprac))./...
    (sqrt(N.*(1+2*snrlinearprac))*(2*variance)));
pdpracor = 1-(1-pdprac).^4;
pdpracand = pdprac.^4;
tmp1 =  (1-pdprac).^2;
tmp2 = (1-pdprac);
pdpracmjr = (6*pdprac.^2).*tmp1+(4*pdprac.^3).*tmp2+pdprac.^4;

pfapracor = 1-(1-pfa).^4;
pfapracand = pfa.^4;
tmp1 =  (1-pfa).^2;
tmp2 = (1-pfa);
pfapracmjr = (6*pfa.^2).*tmp1+(4*pfa.^3).*tmp2+pfa.^4;

%% ROC Characteristics...
figure(1)
hold on;
grid on;
plot(pfapracor,pdpracor(:,5),'-->','LineWidth',2,'MarkerFaceColor','auto');
plot(pfapracor,pdpracor(:,7),'-->','LineWidth',2,'MarkerFaceColor','auto');
plot(pfapracand,pdpracand(:,5),'-d','LineWidth',2,'MarkerFaceColor','auto');
plot(pfapracand,pdpracand(:,7),'-d','LineWidth',2,'MarkerFaceColor','auto');
plot(pfapracmjr,pdpracmjr(:,5),'--','LineWidth',2,'MarkerFaceColor','auto');
plot(pfapracmjr,pdpracmjr(:,7),'--','LineWidth',2,'MarkerFaceColor','auto');
xlabel('Average Probability Of False Alarm');
ylabel('Average Probability of Detection');
title('ROC Characterisitcs of Hard Decision Combining');
hold off;
set(gca,'fontsize',30,'box','on','LineWidth',2,'GridLineStyle','--','GridAlpha'
    ,0.7);
lgd = legend('OR SNR=-10.35dB','OR SNR=-5.3dB','AND SNR=-10.35dB',...
    'AND SNR=-5.3dB','Majority SNR=-10.35dB','Majority SNR=-5.3dB');
lgd.FontSize=20;

%% Probability of detection
figure(2)
hold on;
```

```
grid on;
plot(snrpracticalavg,pdpracor,'->','LineWidth',2);
plot(snrpracticalavg,pdpracand,'-<','LineWidth',2);
plot(snrpracticalavg,pdpracmjr,'-d','LineWidth',2);
xlabel('SNR_{avg} in (dB)');
ylabel('Average Probability of Detection');
title('P_{davg} vs SNR_{avg} for Hard Decision Combining');
hold off;
set(gca,'fontsize',30,'box','on','LineWidth',2,'GridLineStyle','--','GridAlpha'
    ,0.7);
lgd = legend('OR Decision','AND Decision','Majority Rule Decision');
lgd.FontSize=20;
axis([-18.23 15.77 0 1])
```

A.2 softharddecisionpd.m

```
% Soft Decision Combining for sensor nodes...
%% Initializing parameters..
close all;
clear all;
N = [100,200,300,400];% Different sum factor
k=4;% Number of Sensor Nodes
variance = [24.025e-9,23.695e-9,25.678e-9,0.0323e-9];
pfa = 0.05;%Probability of false alarm
for i=1:4
threshold(i) = (qfuncinv(pfa)+sqrt(N(i)))*sqrt(N(i))*2*variance(i);
end
% SNR Values from four sensor nodes
snrpractical = [-21.45,-18.23,-15.45,-13.3,-12.67,-9.35,-2.23,-4.32,2.98,6.95,13
    .57,21.78;...
                -22.23,-20.22,-17.34,-15.32,-13.45,-11.27,-7.75,-5.67,2.53,4.78
                    ,12.67,20.32;...
                -25.34,-23.34,-21.67,-20.33,-16.76,-13.38,-8.56,-6.53,0.38,1.34
                    ,7.89,16.54;...
                -27.32,-24.97,-22.34,-22.23,-17.34,-14.32,-11.35,-7.85,-2.35,-0
```

```
                    .98,2.38,5.98];
for i=1:4
    snrlinearprac(i,:) = 10.^(snrpractical(i,:)/10);
end
for i=1:4
pdprac(i,:) = qfunc((threshold(i)-2*N(i)*variance(i).*(1+snrlinearprac(i,:)))./
    ...
    (sqrt(N(i)*(1+2*snrlinearprac(i,:)))*(2*variance(i))));
end
for i=1:12
snravg(i) = mean(snrpractical(:,i));
end
%% MNE based CS..
pdpracmne = 1-(1-pdprac(1,:)).*(1-pdprac(2,:)).*(1-pdprac(3,:)).*(1-pdprac(4,:))
    ;
pdpracand = mean(pdprac).^4;
pdpracm = mean(pdprac);
pdpracor = 1-(1-pdpracm).^4;
tmp1 =  (1-pdpracm).^(k-2);
tmp2 = (1-pdpracm);
pdpracmjr = (6*pdpracm.^(k-2)).*tmp1+(4*pdpracm.^(k-1)).*tmp2+pdpracm.^k;
figure(1)
hold on;
grid on;
plot(snravg,pdpracmne,'-<','LineWidth',2,'MarkerFaceColor','auto');
axis([-20 10 0 1])
%% EGC based CS..
snrlinearmean = 10.^(snravg/10);
snrlinear = 10.^(snrpractical/10);
pfa = 0.01;
M= mean(N);
threshold = mean(threshold);
for i=1:length(snravg)
    num(i) = threshold-snrlinearmean(i);
    den(i) = (1/16)*((1+2*snrlinear(1,i))/N(1)+variance(1)+(1+2*snrlinear(2,i))/
       N(2)+variance(2)+(1+2*snrlinear(3,i))/N(3)+variance(3)+(1+2*snrlinear(4,
       i))/N(4)+variance(4));
```

```
    pdegc(i) = qfunc(num(i)/sqrt(den(i)));
end

%% Plotting the data..
plot(snravg,pdegc,'-d','LineWidth',2,'MarkerFaceColor','auto');
plot(snravg,pdpracand,'-s','LineWidth',2,'MarkerFaceColor','auto');
plot(snravg,pdpracor,'-s','LineWidth',2,'MarkerFaceColor','auto');
plot(snravg,pdpracmjr,'->','LineWidth',2,'MarkerFaceColor','auto');
title('P_{davg} vs SNR_{avg} for Soft and Hard Decision Combining');
xlabel('SNR_{avg} in (dB)');
ylabel('Average Probability of Detection');
set(gca,'fontsize',30,'box','on','LineWidth',2,'GridLineStyle','--','GridAlpha'
    ,0.7);
legend('MNE Combining','EGC Combining','AND Rule','OR Rule','Majority Rule');
```

A.3 spectrumsenseusrp.py

```
#!/usr/bin/env python
#
# Copyright 2005,2007,2011 Free Software Foundation, Inc.
#
# This file is part of GNU Radio
#
# GNU Radio is free software; you can redistribute it and/or modify
# it under the terms of the GNU General Public License as published by
# the Free Software Foundation; either version 3, or (at your option)
# any later version.
#
# GNU Radio is distributed in the hope that it will be useful,
# but WITHOUT ANY WARRANTY; without even the implied warranty of
# MERCHANTABILITY or FITNESS FOR A PARTICULAR PURPOSE.  See the
# GNU General Public License for more details.
#
# You should have received a copy of the GNU General Public License
# along with GNU Radio; see the file COPYING.  If not, write to
```

```
# the Free Software Foundation, Inc., 51 Franklin Street,
# Boston, MA 02110-1301, USA.
#

from gnuradio import gr, eng_notation
from gnuradio import blocks
from gnuradio import audio
from gnuradio import filter
from gnuradio import fft
from gnuradio import uhd
from gnuradio.eng_option import eng_option
from optparse import OptionParser
import sys
import math
import struct
import threading
from datetime import datetime
import time
from gnuradio.wxgui import stdgui2, fftsink2, form
import wx

sys.stderr.write("Warning: this may have issues on some machines+Python version
   combinations to seg fault due to the callback in bin_statitics.\n\n")

class ThreadClass(threading.Thread):
    def run(self):
        return

class tune(gr.feval_dd):
    """
    This class allows C++ code to callback into python.
    """
    def __init__(self, tb):
        gr.feval_dd.__init__(self)
        self.tb = tb

    def eval(self, ignore):
```

```
        """
        This method is called from blocks.bin_statistics_f when it wants
        to change the center frequency.  This method tunes the front
        end to the new center frequency, and returns the new frequency
        as its result.
        """

        try:
            new_freq = self.tb.set_next_freq()
            while(self.tb.msgq.full_p()):
                time.sleep(0.1)
            return new_freq

        except Exception, e:
            print "tune: Exception: ", e


class parse_msg(object):
    def __init__(self, msg):
        self.center_freq = msg.arg1()
        self.vlen = int(msg.arg2())
        assert(msg.length() == self.vlen * gr.sizeof_float)
        t = msg.to_string()
        self.raw_data = t
        self.data = struct.unpack('%df' % (self.vlen,), t)


class my_top_block(gr.top_block):

    def __init__(self):
        gr.top_block.__init__(self)

        usage = "usage: %prog [options] min_freq max_freq"
        parser = OptionParser(option_class=eng_option, usage=usage)
        parser.add_option("-a", "--args", type="string", default="",
                          help="UHD device device address args [default=%default
                            ]")
```

```
parser.add_option("", "--spec", type="string", default=None,
              help="Subdevice of UHD device where appropriate")
parser.add_option("-A", "--antenna", type="string", default=None,
                  help="select Rx Antenna where appropriate")
parser.add_option("-s", "--samp-rate", type="eng_float", default=1e6,
                  help="set sample rate [default=%default]")
parser.add_option("-g", "--gain", type="eng_float", default=None,
                  help="set gain in dB (default is midpoint)")
parser.add_option("", "--tune-delay", type="eng_float",
                  default=0.25, metavar="SECS",
                  help="time to delay (in seconds) after changing
                      frequency [default=%default]")
parser.add_option("", "--dwell-delay", type="eng_float",
                  default=0.25, metavar="SECS",
                  help="time to dwell (in seconds) at a given frequency
                      [default=%default]")
parser.add_option("-b", "--channel-bandwidth", type="eng_float",
                  default=6.25e3, metavar="Hz",
                  help="channel bandwidth of fft bins in Hz [default=%
                      default]")
parser.add_option("-l", "--lo-offset", type="eng_float",
                  default=0, metavar="Hz",
                  help="lo_offset in Hz [default=%default]")
parser.add_option("-q", "--squelch-threshold", type="eng_float",
                  default=None, metavar="dB",
                  help="squelch threshold in dB [default=%default]")
parser.add_option("-F", "--fft-size", type="int", default=None,
                  help="specify number of FFT bins [default=samp_rate/
                      channel_bw]")
parser.add_option("", "--real-time", action="store_true", default=False,
                  help="Attempt to enable real-time scheduling")

(options, args) = parser.parse_args()
if len(args) != 2:
    parser.print_help()
    sys.exit(1)
```

```
self.channel_bandwidth = options.channel_bandwidth

self.min_freq = eng_notation.str_to_num(args[0])
self.max_freq = eng_notation.str_to_num(args[1])

if self.min_freq > self.max_freq:
    # swap them
    self.min_freq, self.max_freq = self.max_freq, self.min_freq

if not options.real_time:
    realtime = False
else:
    # Attempt to enable realtime scheduling
    r = gr.enable_realtime_scheduling()
    if r == gr.RT_OK:
        realtime = True
    else:
        realtime = False
        print "Note: failed to enable realtime scheduling"

# build graph
self.u = uhd.usrp_source(device_addr=options.args,
                         stream_args=uhd.stream_args('fc32'))

# Set the subdevice spec
if(options.spec):
    self.u.set_subdev_spec(options.spec, 0)

# Set the antenna
if(options.antenna):
    self.u.set_antenna(options.antenna, 0)

self.u.set_samp_rate(options.samp_rate)
self.usrp_rate = usrp_rate = self.u.get_samp_rate()

self.lo_offset = options.lo_offset
```

```
    if options.fft_size is None:
        self.fft_size = int(self.usrp_rate/self.channel_bandwidth)
    else:
        self.fft_size = options.fft_size

    self.squelch_threshold = options.squelch_threshold

    s2v = blocks.stream_to_vector(gr.sizeof_gr_complex, self.fft_size)

    mywindow = filter.window.blackmanharris(self.fft_size)
    ffter = fft.fft_vcc(self.fft_size, True, mywindow, True)
    power = 0
    for tap in mywindow:
        power += tap*tap
    c2mag = blocks.complex_to_mag_squared(self.fft_size)
    self.freq_step = self.nearest_freq((0.75 * self.usrp_rate),
        self.channel_bandwidth)
    self.min_center_freq = self.min_freq + (self.freq_step/2)
    nsteps = math.ceil((self.max_freq - self.min_freq) / self.freq_step)
    self.max_center_freq = self.min_center_freq + (nsteps * self.freq_step)
    self.next_freq = self.min_center_freq
    tune_delay  = max(0, int(round(options.tune_delay * usrp_rate /
        self.fft_size)))  # in fft_frames
    dwell_delay = max(1, int(round(options.dwell_delay * usrp_rate /
        self.fft_size))) # in fft_frames
    self.msgq = gr.msg_queue(1)
    self._tune_callback = tune(self)        # hang on to this to keep it
        from being GC'd
    stats = blocks.bin_statistics_f(self.fft_size, self.msgq,
                                    self._tune_callback, tune_delay,
                                    dwell_delay)
self.connect(self.u, s2v, ffter, c2mag, stats)

    if options.gain is None:

        g = self.u.get_gain_range()
        options.gain = float(g.start()+g.stop())/2.0
```

```
        self.set_gain(options.gain)
        print "gain =", options.gain

    def set_next_freq(self):
        target_freq = self.next_freq
        self.next_freq = self.next_freq + self.freq_step
        if self.next_freq >= self.max_center_freq:
            self.next_freq = self.min_center_freq

        if not self.set_freq(target_freq):
            print "Failed to set frequency to", target_freq
            sys.exit(1)

        return target_freq


    def set_freq(self, target_freq):
        """
        Set the center frequency we're interested in.

        Args:
            target_freq: frequency in Hz
        @rypte: bool
        """

        r = self.u.set_center_freq(uhd.tune_request(target_freq, rf_freq=(
            target_freq + self.lo_offset),rf_freq_policy=
            uhd.tune_request.POLICY_MANUAL))
        if r:
            return True

        return False

    def set_gain(self, gain):
        self.u.set_gain(gain)
```

```
    def nearest_freq(self, freq, channel_bandwidth):
        freq = round(freq / channel_bandwidth, 0) * channel_bandwidth
        return freq

def main_loop(tb):

    def bin_freq(i_bin, center_freq):
        freq = center_freq - (tb.usrp_rate / 2) + (tb.channel_bandwidth * i_bin)
        return freq

    bin_start = int(tb.fft_size * ((1 - 0.25) / 2))
    bin_stop = int(tb.fft_size - bin_start)
    fid = open("./usrp.dat","wb")
    while 1:
    m = parse_msg(tb.msgq.delete_head())
        for i_bin in range(bin_start, bin_stop):
            center_freq = m.center_freq
            freq = bin_freq(i_bin, center_freq)
        power_db = 10*math.log10(m.data[i_bin]/tb.usrp_rate)
        signal = m.data[i_bin]/(tb.usrp_rate)

            if (power_db > tb.squelch_threshold) and (freq >= tb.min_freq) and (
                freq <= tb.max_freq):
        print freq,signal,power_db
        fid.write(struct.pack('<f',signal))
    fid.close()#closing the file

if __name__ == '__main__':
    t = ThreadClass()
    t.start()

    tb = my_top_block()
    try:
        tb.start()
        main_loop(tb)

    except KeyboardInterrupt:
```

```
        pass
```

A.4 gnuradiortlsdrsense.py

```
#!/usr/bin/env python2
# -*- coding: utf-8 -*-
##################################################
# GNU Radio Python Flow Graph
# Title: DTv Spectrum Sensing
# Author: Gill
# Description: Frequency Sweep for UHF White Spaces
# Generated: Fri Mar 10 14:30:20 2017
##################################################

if __name__ == '__main__':
    import ctypes
    import sys
    if sys.platform.startswith('linux'):
        try:
            x11 = ctypes.cdll.LoadLibrary('libX11.so')
            x11.XInitThreads()
        except:
            print "Warning: failed to XInitThreads()"

from PyQt4 import Qt
from gnuradio import blocks
from gnuradio import eng_notation
from gnuradio import fft
from gnuradio import gr
from gnuradio import qtgui
from gnuradio.eng_option import eng_option
from gnuradio.fft import window
from gnuradio.filter import firdes
from optparse import OptionParser
import numpy as np
```

```
import osmosdr
import sip
import sys
import time


class spectrum_sensing(gr.top_block, Qt.QWidget):

    def __init__(self):
        gr.top_block.__init__(self, "DTv Spectrum Sensing")
        Qt.QWidget.__init__(self)
        self.setWindowTitle("DTv Spectrum Sensing")
        try:
            self.setWindowIcon(Qt.QIcon.fromTheme('gnuradio-grc'))
        except:
            pass
        self.top_scroll_layout = Qt.QVBoxLayout()
        self.setLayout(self.top_scroll_layout)
        self.top_scroll = Qt.QScrollArea()
        self.top_scroll.setFrameStyle(Qt.QFrame.NoFrame)
        self.top_scroll_layout.addWidget(self.top_scroll)
        self.top_scroll.setWidgetResizable(True)
        self.top_widget = Qt.QWidget()
        self.top_scroll.setWidget(self.top_widget)
        self.top_layout = Qt.QVBoxLayout(self.top_widget)
        self.top_grid_layout = Qt.QGridLayout()
        self.top_layout.addLayout(self.top_grid_layout)

        self.settings = Qt.QSettings("GNU Radio", "spectrum_sensing")
        self.restoreGeometry(self.settings.value("geometry").toByteArray())

        ##################################################
        # Variables
        ##################################################
        self.samp_rate = samp_rate = int(2e6)
        self.freq = freq = 450e6
        self.N = N = 1000
```

```
##################################################
# Blocks
##################################################
self.rtlsdr_source_0 = osmosdr.source( args="numchan=" + str(1) + " " +
    '' )
self.rtlsdr_source_0.set_time_source('external', 0)
self.rtlsdr_source_0.set_sample_rate(samp_rate)
self.rtlsdr_source_0.set_center_freq(freq, 0)
self.rtlsdr_source_0.set_freq_corr(0, 0)
self.rtlsdr_source_0.set_dc_offset_mode(2, 0)
self.rtlsdr_source_0.set_iq_balance_mode(0, 0)
self.rtlsdr_source_0.set_gain_mode(True, 0)
self.rtlsdr_source_0.set_gain(15, 0)
self.rtlsdr_source_0.set_if_gain(15, 0)
self.rtlsdr_source_0.set_bb_gain(15, 0)
self.rtlsdr_source_0.set_antenna('', 0)
self.rtlsdr_source_0.set_bandwidth(0, 0)

self.qtgui_freq_sink_x_0 = qtgui.freq_sink_c(
    1024, #size
    firdes.WIN_BLACKMAN_hARRIS, #wintype
    0, #fc
    samp_rate, #bw
    "Recieved Signal", #name
    1 #number of inputs
)
self.qtgui_freq_sink_x_0.set_update_time(0.10)
self.qtgui_freq_sink_x_0.set_y_axis(-120, 0)
self.qtgui_freq_sink_x_0.set_y_label('Relative Gain', 'dB')
self.qtgui_freq_sink_x_0.set_trigger_mode(qtgui.TRIG_MODE_FREE, 0.0, 0,
    "")
self.qtgui_freq_sink_x_0.enable_autoscale(True)
self.qtgui_freq_sink_x_0.enable_grid(True)
self.qtgui_freq_sink_x_0.set_fft_average(1.0)
self.qtgui_freq_sink_x_0.enable_axis_labels(True)
self.qtgui_freq_sink_x_0.enable_control_panel(False)
```

```
if not True:
  self.qtgui_freq_sink_x_0.disable_legend()

if "complex" == "float" or "complex" == "msg_float":
  self.qtgui_freq_sink_x_0.set_plot_pos_half(not True)

labels = ['', '', '', '', '',
          '', '', '', '', '']
widths = [2, 1, 1, 1, 1,
          1, 1, 1, 1, 1]
colors = ["blue", "red", "green", "black", "cyan",
          "magenta", "yellow", "dark red", "dark green", "dark blue"]
alphas = [1.0, 1.0, 1.0, 1.0, 1.0,
          1.0, 1.0, 1.0, 1.0, 1.0]
for i in xrange(1):
    if len(labels[i]) == 0:
        self.qtgui_freq_sink_x_0.set_line_label(i, "Data {0}".format(i))
    else:
        self.qtgui_freq_sink_x_0.set_line_label(i, labels[i])
    self.qtgui_freq_sink_x_0.set_line_width(i, widths[i])
    self.qtgui_freq_sink_x_0.set_line_color(i, colors[i])
    self.qtgui_freq_sink_x_0.set_line_alpha(i, alphas[i])

self._qtgui_freq_sink_x_0_win = sip.wrapinstance(
    self.qtgui_freq_sink_x_0.pyqwidget(), Qt.QWidget)
self.top_layout.addWidget(self._qtgui_freq_sink_x_0_win)
self.fft_vxx_0 = fft.fft_vcc(1024, True, (window.blackmanharris(1024)),
    True, 1)
self.blocks_vector_to_stream_0 = blocks.vector_to_stream(gr.sizeof_float
    *1, 1024)
self.blocks_stream_to_vector_0 = blocks.stream_to_vector(
    gr.sizeof_gr_complex*1, 1024)
self.blocks_moving_average_xx_0 = blocks.moving_average_ff(N, 1, 4000)
self.blocks_file_sink_2_0 = blocks.file_sink(gr.sizeof_float*1, '/home/
    gill/Desktop/ms-thesis/gr-spectrumsensing/grc/rtl-sdr_sensing/
    Results/snr_check.dat', False)
```

```
        self.blocks_file_sink_2_0.set_unbuffered(False)
        self.blocks_complex_to_mag_squared_0 = blocks.complex_to_mag_squared
            (1024)

        ##################################################
        # Connections
        ##################################################
        self.connect((self.blocks_complex_to_mag_squared_0, 0), (
            self.blocks_vector_to_stream_0, 0))
        self.connect((self.blocks_moving_average_xx_0, 0), (
            self.blocks_file_sink_2_0, 0))
        self.connect((self.blocks_stream_to_vector_0, 0), (self.fft_vxx_0, 0))
        self.connect((self.blocks_vector_to_stream_0, 0), (
            self.blocks_moving_average_xx_0, 0))
        self.connect((self.fft_vxx_0, 0), (self.blocks_complex_to_mag_squared_0,
             0))
        self.connect((self.rtlsdr_source_0, 0), (self.blocks_stream_to_vector_0,
             0))
        self.connect((self.rtlsdr_source_0, 0), (self.qtgui_freq_sink_x_0, 0))

    def closeEvent(self, event):
        self.settings = Qt.QSettings("GNU Radio", "spectrum_sensing")
        self.settings.setValue("geometry", self.saveGeometry())
        event.accept()

    def get_samp_rate(self):
        return self.samp_rate

    def set_samp_rate(self, samp_rate):
        self.samp_rate = samp_rate
        self.rtlsdr_source_0.set_sample_rate(self.samp_rate)
        self.qtgui_freq_sink_x_0.set_frequency_range(0, self.samp_rate)

    def get_freq(self):
        return self.freq

    def set_freq(self, freq):
```

```
        self.freq = freq
        self.rtlsdr_source_0.set_center_freq(self.freq, 0)

    def get_N(self):
        return self.N

    def set_N(self, N):
        self.N = N
        self.blocks_moving_average_xx_0.set_length_and_scale(self.N, 1)


def main(top_block_cls=spectrum_sensing, options=None):

    from distutils.version import StrictVersion
    if StrictVersion(Qt.qVersion()) >= StrictVersion("4.5.0"):
        style = gr.prefs().get_string('qtgui', 'style', 'raster')
        Qt.QApplication.setGraphicsSystem(style)
    qapp = Qt.QApplication(sys.argv)

    tb = top_block_cls()
    tb.start()
    tb.show()

    def quitting():
        tb.stop()
        tb.wait()
    qapp.connect(qapp, Qt.SIGNAL("aboutToQuit()"), quitting)
    qapp.exec_()


if __name__ == '__main__':
    main()
```

Appendix B

LTE-R Analysis Code

B.1 kfactordist.m

```
% Calculating K-factor for the tunnel environment for HST
clear all;
close all;
clc;
%% Creating a doppler profile for high speed raiway scenario..
Ds = 30;%Initial Distance between tx and rx times 2..
Dmin = 2;% Distance between raiway tracks and leaky feeder cables...
Kf = [];
fc = 3e9;%center frequency..
c = 3e8;
v = 138.9;%300;
t = linspace(0,(2*Ds)/v(1),100);
fd = (v*fc)/3e8;%maximum doppler frequency...
costheta = zeros(size(t));%angle between BS and MS
d1 = [];
for i=1:length(t)
    d1(i) = sqrt(2^2+(Ds/2-v(1)*t(i))^2);%distance between tx and rx..
    if t(i) >=0 && t(i)<= (Ds/v)
        costheta(i) = ((Ds/2)-v*t(i))./sqrt(Dmin^2+(Ds/2-v*t(i))^2);
```

```
    elseif t(i) > (Ds/v) && t(i)<=(2*Ds)/v
        costheta(i) = (-1.5*Ds+v*t(i))./sqrt(Dmin^2+(-1.5*Ds+v*t(i))^2);
    end
end
fs  = fd*costheta;
thetadeg = acosd(costheta);
fc_wds = fc-fs;
lambda = c./fc_wds;
Cin = 5-((0.1*1.8e10)./fc_wds)*1j;
C = Cin;
gammanum = C.*sind(thetadeg)-sqrt(Cin-(cosd(thetadeg)).^2);
gammaden = C.*sind(thetadeg)+sqrt(Cin-(cosd(thetadeg)).^2);
gamma = gammanum./gammaden;
ht = 6.1;%height of feeder cable
hr = 4.2;%height of the train
var1 = sqrt(d1.^2+(ht+hr)^2);
var2 = sqrt(d1.^2+(ht-hr)^2);
phase = ((((2*pi)./lambda).*(var1-var2))*180)/pi;
gammad = atan2d(imag(gamma),real(gamma));
phasegamma = abs(cosd(gammad-phase));
K = abs(gamma).^2+2*abs(gamma).*phasegamma;
Kf = 10*log10(1./K);
```

B.2 bercalculation.m

```
% Demonstration of Eb/N0 Vs SER for M-QAM modulation scheme
clc;
load Kf;
load t;
%---------Input Fields------------------------
%% QPSk
bitsperframe=1e3; %Number of input symbols
EbN0dB = [linspace(0,20,50) fliplr(linspace(0,20,50))]; %Define EbN0dB range for
     simulation
M=4; %for QPSk modulation.
```

```
hMod = comm.RectangularQAMModulator('ModulationOrder',M);
const = step(hMod,(0:3)');
%---------------------------------------------
refArray =1/sqrt(2)*const';
k=log2(M);
totPower=15; %Total power of LOS path & scattered paths

EsN0dB = EbN0dB + 10*log10(k);
biterrsim = zeros(size(EsN0dB));
%---Generating a uniformly distributed random numbers in the set [0,1,2,..,M-1]
data=ceil(M.*rand(bitsperframe,1))-1;
s=refArray(data+1); %QPSK Constellation mapping with Gray coding
%--- Reference Constellation for demodulation and Error rate computation--
refI = real(refArray);
refQ = imag(refArray);
%---Place holder for Symbol Error values for each Es/N0 for particular M value--
index=1;
u=1;
% Kf = 4.9;
K = 10.^(Kf/10);
for x=EsN0dB
    sn=sqrt(K(u)/(K(u)+1)*totPower); %Non-Centrality Parameter
    sigma=totPower/sqrt(2*(K(u)+1));
    h=((sigma*randn(1,bitsperframe)+sn)+1i*(randn(1,bitsperframe)*sigma+0));
    numerr = 0;
    numBits = 0;
    while numerr < 100 && numBits < 1e7
        %---------------------------------------------
        %Channel Noise for various Es/N0
        %---------------------------------------------
        %Adding noise with variance according to the required Es/N0
        noiseVariance = 1/(10.^(x/10));%Standard deviation for AWGN Noise
        noiseSigma = sqrt(noiseVariance/2);
        %Creating a complex noise for adding with M-QAM modulated signal
        %Noise is complex since M-QAM is in complex representation
        noise = noiseSigma*(randn(size(s))+1i*randn(size(s)));
        received = s.*h + noise;
```

```
        %-------------I-Q Branching---------------
        received = received./h;
        r_i = real(received);
        r_q = imag(received);
        %---Decision Maker-Compute (r_i-s_i)^2+(r_q-s_q)^2 and choose the
            smallest
        r_i_repmat = repmat(r_i,M,1);
        r_q_repmat = repmat(r_q,M,1);
        distance = zeros(M,bitsperframe); %place holder for distance metric
        minDistIndex=zeros(bitsperframe,1);
            for j=1:bitsperframe
            %---Distance computation - (r_i-s_i)^2+(r_q-s_q)^2 --------------
            distance(:,j) = (r_i_repmat(:,j)-refI').^2+(r_q_repmat(:,j)-refQ').
                ^2;
            %---capture the index in the array where the minimum distance occurs
            [dummy,minDistIndex(j)]=min(distance(:,j));
            end
        y = minDistIndex - 1;
        %--------------Symbol Error Rate Calculation
            -------------------------------
        dataCap = y;
        numerr = sum(dataCap~=data)+numerr;
        numBits = numBits+bitsperframe;
        disp(numerr);
    end
symErrSimulatedqpsk(1,index) = numerr/numBits;
biterrsim(1,index) = symErrSimulatedqpsk(1,index)/k;
index=index+1;
% u=u+1;
end

%% 16 QAM
bitsperframe=1e3; %Number of input symbols
EbN0dB = [linspace(0,10,50) fliplr(linspace(0,10,50))]; %Define EbN0dB range for
     simulation
M=16; %for QPSk modulation.
hMod = comm.RectangularQAMModulator('ModulationOrder',M);
```

```
const = step(hMod,(0:M-1)');
%------------------------------------------------
refArray =1/sqrt(10)*const';
k=log2(M);
totPower=10; %Total power of LOS path & scattered paths


EsN0dB = EbN0dB + 10*log10(k);
biterrsim = zeros(size(EsN0dB));
%---Generating a uniformly distributed random numbers in the set [0,1,2,..,M-1]
data=ceil(M.*rand(bitsperframe,1))-1;
s=refArray(data+1); %QPSK Constellation mapping with Gray coding
%--- Reference Constellation for demodulation and Error rate computation--
refI = real(refArray);
refQ = imag(refArray);
%---Place holder for Symbol Error values for each Es/N0 for particular M value--
index=1;
u=1;
K = 10.^(Kf/10);
for x=EsN0dB
    numerr = 0;
    numBits = 0;
    while numerr < 100 && numBits < 1e7
        sn=sqrt(K(u)/(K(u)+1)*totPower); %Non-Centrality Parameter
        sigma=totPower/sqrt(2*(K(u)+1));
        h=((sigma*randn(1,bitsperframe)+sn)+1i*(randn(1,bitsperframe)*sigma+0));
        %--------------------------------------------
        %Channel Noise for various Es/N0
        %--------------------------------------------
        %Adding noise with variance according to the required Es/N0
        noiseVariance = 1/(10.^(x/10));%Standard deviation for AWGN Noise
        noiseSigma = sqrt(noiseVariance/2);
        %Creating a complex noise for adding with M-QAM modulated signal
        %Noise is complex since M-QAM is in complex representation
        noise = noiseSigma*(randn(size(s))+1i*randn(size(s)));
        received = s.*h + noise;
        %-------------I-Q Branching---------------
```

```
        received = received./h;
        r_i = real(received);
        r_q = imag(received);
        %---Decision Maker-Compute (r_i-s_i)^2+(r_q-s_q)^2 and choose the
            smallest
        r_i_repmat = repmat(r_i,M,1);
        r_q_repmat = repmat(r_q,M,1);
        distance = zeros(M,bitsperframe); %place holder for distance metric
        minDistIndex=zeros(bitsperframe,1);
            for j=1:bitsperframe
            %---Distance computation - (r_i-s_i)^2+(r_q-s_q)^2 --------------
            distance(:,j) = (r_i_repmat(:,j)-refI').^2+(r_q_repmat(:,j)-refQ').
                ^2;
            %---capture the index in the array where the minimum distance occurs
            [dummy,minDistIndex(j)]=min(distance(:,j));
            end
        y = minDistIndex - 1;
        %--------------Symbol Error Rate Calculation
            -------------------------------
        dataCap = y;
        numerr = sum(dataCap~=data)+numerr;
        numBits = numBits+bitsperframe;
        disp(numerr);
    end
symErrSimulatedqam(1,index) = numerr/numBits;
biterrsim(1,index) = symErrSimulatedqam(1,index)/k;
index=index+1;
u=u+1;
end

%% 64 QAM Modulation...
bitsperframe=1e3; %Number of input symbols
EbN0dB = [linspace(0,10,50) fliplr(linspace(0,10,50))]; %Define EbN0dB range for
     simulation
M=64; %for QPSk modulation.
hMod = comm.RectangularQAMModulator('ModulationOrder',M);
const = step(hMod,(0:M-1)');
```

```
%---------------------------------------------
refArray =1/sqrt(42)*const';
k=log2(M);
totPower=10; %Total power of LOS path & scattered paths
EsN0dB = EbN0dB + 10*log10(k);
biterrsim = zeros(size(EsN0dB));
%---Generating a uniformly distributed random numbers in the set [0,1,2,..,M-1]
data=ceil(M.*rand(bitsperframe,1))-1;
s=refArray(data+1); %QPSK Constellation mapping with Gray coding
%--- Reference Constellation for demodulation and Error rate computation--
refI = real(refArray);
refQ = imag(refArray);
%---Place holder for Symbol Error values for each Es/N0 for particular M value--
index=1;
u=1;
K = 10.^(Kf/10);
for x=EsN0dB
     sn=sqrt(K(u)/(K(u)+1)*totPower); %Non-Centrality Parameter
     sigma=totPower/sqrt(2*(K(u)+1));
     h=((sigma*randn(1,bitsperframe)+sn)+1i*(randn(1,bitsperframe)*sigma+0));
     numerr = 0;
     numBits = 0;
    while numerr < 100 && numBits < 1e7
        %--------------------------------------------
        %Channel Noise for various Es/N0
        %--------------------------------------------
        %Adding noise with variance according to the required Es/N0
        noiseVariance = 1/(10.^(x/10));%Standard deviation for AWGN Noise
        noiseSigma = sqrt(noiseVariance/2);
        %Creating a complex noise for adding with M-QAM modulated signal
        %Noise is complex since M-QAM is in complex representation
        noise = noiseSigma*(randn(size(s))+1i*randn(size(s)));
        received = s.*h + noise;
        %-------------I-Q Branching---------------
        received = received./h;
        r_i = real(received);
        r_q = imag(received);
```

```
        %---Decision Maker-Compute (r_i-s_i)^2+(r_q-s_q)^2 and choose the
            smallest
        r_i_repmat = repmat(r_i,M,1);
        r_q_repmat = repmat(r_q,M,1);
        distance = zeros(M,bitsperframe); %place holder for distance metric
        minDistIndex=zeros(bitsperframe,1);
            for j=1:bitsperframe
            %---Distance computation - (r_i-s_i)^2+(r_q-s_q)^2 --------------
            distance(:,j) = (r_i_repmat(:,j)-refI').^2+(r_q_repmat(:,j)-refQ').
                ^2;
            %---capture the index in the array where the minimum distance occurs
            [dummy,minDistIndex(j)]=min(distance(:,j));
            end
        y = minDistIndex - 1;
        %--------------Symbol Error Rate Calculation
            -------------------------------
        dataCap = y;
        numerr = sum(dataCap~=data)+numerr;
        numBits = numBits+bitsperframe;
        disp(numerr);
    end
symErrSimulatedqam64(1,index) = numerr/numBits;
biterrsim(1,index) = symErrSimulatedqam64(1,index)/k;
index=index+1;
u=u+1;
end

%%
fig = figure;
semilogy(t*1e3,symErrSimulatedqpsk(1,:),'-d','LineWidth',2);
hold on;
grid on;
semilogy(t*1e3,symErrSimulatedqam(1,:),'-d','LineWidth',2);
semilogy(t*1e3,symErrSimulatedqam64(1,:),'-d','LineWidth',2);
xlabel('Time (ms)');
ylabel('Bit Error Rate (Pb)');
title(['BER For OFDM Under Rician Fading Environment Inside Tunnel']);
```

```
set(gca,'fontsize',30,'box','on','LineWidth',2,'GridLineStyle','--','GridAlpha'
    ,0.7);
axis([0 max(t)*1e3 10e-7 0])
lgd = legend('QPSK','16QAM','64QAM');
lgd.FontSize=20;
```